Title: Cell type-specific gene expression dynamics during human brain maturation

Christina Steyn[1,2], Ruvimbo Mishi[1,2], Stephanie Fillmore[1,2], Matthijs B. Verhoog[1,2], Jessica More[1,2], Ursula K. Rohlwink[2,3], Roger Melvill[3], James Butler[2,4], Johannes M. N. Enslin[2,3], Muazzam Jacobs[2,5,6,7], Tatjana Sauka-Spengler[8,9], Maria Greco[10], Sadi Quiñones[11,12], Chris G. Dulla[11], Joseph V. Raimondo[1,2,5], Anthony Figaji[2,3] and Dorit Hockman[1,2,*]

Affiliations:

[1]Division of Cell Biology, Department of Human Biology, University of Cape Town, Cape Town, South Africa

[2]Neuroscience Institute, University of Cape Town, Cape Town, South Africa

[3]Division of Neurosurgery, Department of Surgery, University of Cape Town, Cape Town, South Africa

[4]Division of Neurology, Department of Medicine, University of Cape Town, Cape Town, South Africa

[5]Institute of Infectious Disease and Molecular Medicine, University of Cape Town, Cape Town, South Africa

[6]Division of Immunology, Department of Pathology University of Cape Town

[7]National Health Laboratory Service, South Africa

[8]Radcliffe Department of Medicine, MRC Weatherall Institute of Molecular Medicine, University of Oxford, Oxford, UK

[9]Stowers Institute for Medical Research, Kansas City, MO, USA

[10]Single Cell Facility, MRC Weatherall Institute of Molecular Medicine, University of Oxford, Oxford, UK

[11]Department of Neuroscience, Graduate School of Biomedical Sciences, Tufts University School of Medicine, Boston, MA, USA

[12]Graduate School of Biomedical Science, Tufts University School of Medicine, Boston, MA, USA

*Corresponding author

Abstract

The human brain undergoes protracted post-natal maturation, guided by dynamic changes in gene expression. Most studies exploring these processes have used bulk tissue analyses, which mask cell type-specific gene expression dynamics. Here, using single nucleus (sn)RNA-seq on temporal lobe tissue, including samples of African ancestry, we build a joint paediatric and adult atlas of 75 cell subtypes, which we verify with spatial transcriptomics. We explore the differences between paediatric and adult cell types, revealing the genes and pathways that change during brain maturation. Our results highlight excitatory neuron subtypes, including the *LTK* and *FREM* subtypes, that show elevated expression of genes associated with cognition and synaptic plasticity in paediatric tissue. The new resources we present here

42 improve our understanding of the brain during its development and contribute to global
43 efforts to build an inclusive brain cell map.
44
45 **Introduction**
46
47 The adult human brain is a complex assembly of diverse cell types, which has been defined
48 with unprecedented accuracy using single cell transcriptomics[1-4]. This adult transcriptomic
49 signature is set up over a protracted period of development, which begins in the embryo and
50 continues after birth. While the single cell diversity of the embryonic human brain has been
51 explored[5,6], little is known about how these cell type-specific gene expression profiles change
52 during childhood[7]. Most existing studies have used bulk transcriptomic approaches, which
53 revealed a dramatic period of global gene expression change during the late foetal/early
54 infancy transition, that stabilises during childhood (1 to <12-years-old) and adolescence (12
55 to <20-years-old)[6,8-11]. Bulk transcriptomics, however, cannot reveal the more subtle, cell
56 type-specific changes in gene expression that drive brain maturation from childhood,
57 through adolescence to adulthood.

58 Childhood and adolescence are periods of important changes in brain structure, during which
59 neuronal connections are refined and strengthened. While synaptogenesis peaks in the early
60 postnatal period, synaptic pruning activity begins during late childhood, peaks during
61 adolescence, and then gradually decreases[12-14]. These stages therefore represent periods of
62 enhanced susceptibility to environmental influence, as well as increased neuropsychiatric
63 risk[15]. Describing the typical cell type-specific gene expression trajectories of the maturing
64 brain will allow us to assess the effects of genetic perturbations and early adverse experiences
65 on brain maturation. Furthermore, investigating the driving forces behind cell type-specific
66 maturational processes may help develop targeted therapies for neurological disease[16].

67 To this end, the Paediatric Cell Atlas (PCA)[17], a branch of the Human Cell Atlas (HCA)[3], aims to
68 ensure that the benefits of single cell transcriptomics are available to children as well as adults
69 from diverse populations[3,17]. Africa has the most genetically diverse[18] and youngest
70 population[19] worldwide and by 2050, 37% of the world's children will grow up in Africa[20].
71 Consequently, it is essential to include the African paediatric population in the PCA's efforts.
72 A reference paediatric brain cell atlas that includes data from African donors will contribute
73 to developing treatments for locally prevalent conditions, such as tuberculosis meningitis
74 (TBM) and HIV[21,22]. In addition, studying the differences in gene expression dynamics between
75 adult and paediatric brains may explain why the manifestation of neurological conditions and
76 responses to therapies differ across the lifespan[17].

77 To contribute to these endeavours, we present a joint paediatric and adult temporal cortex
78 cell atlas, including samples from eight Southern African donors, annotated using the Allen
79 Brain Map middle temporal gyrus (MTG) cell taxonomy[1]. We validate our annotation using
80 spatial transcriptomics analysis. In addition, we use *de novo* marker gene analysis with

machine learning tools to compare our paediatric and adult datasets to the existing MTG cell taxonomy and compare markers that define paediatric versus adult cell states. Using differential gene expression analysis, we highlight 21 cell subtypes that show differential expression of genes involved in neurodevelopment and cognition. Finally, we use our datasets to define the cell type-specific gene expression of putative site-of-disease TBM biomarkers[23]. Overall, we highlight the subtle cell type-specific differences between the paediatric and adult brain and expand the representation of diverse paediatric populations in the HCA.

Results

A joint paediatric and adult temporal cortex cell atlas

We generated snRNA-seq libraries from five paediatric and three adult donor temporal cortex tissue samples. The majority of our samples were obtained from surgeries to treat epilepsy (Extended Data Table 1). These new libraries were analysed alongside similar published datasets[24], resulting in a total of 23 snRNA-seq datasets (including technical replicates) from 12 individuals (six paediatric and six adult) (Fig. 1a). The samples were sequenced to a median depth of 19,853 reads per nucleus, with 176,012 nuclei remaining after removing low quality barcodes (Extended Data Fig. 1, Extended Data Table 2). While our new datasets had a lower average sequencing depth than the co-analysed published datasets, the average number of genes and transcripts detected across datasets was similar (Extended Data Table 2).

Using data integration and clustering we aligned similar cell types across the 23 datasets, yielding 40 clusters (Fig. 1a, Extended Data Fig. 1i-h). Each cluster was assigned to one of the major brain cell types (level 1 annotation) based on marker gene expression (Extended Data Fig. 2a, Extended Data Table 3, Supplementary Figure 1). Additionally, we used label transfer[25] to classify each nucleus according to the Allen Brain Map MTG atlas[1] (level 2 annotation) (Extended Data Table 3). Barcodes with discordant level 1 and level 2 annotations (17.94%) were removed to focus downstream analyses on nuclei with high confidence annotations (Extended Data Table 3). Based on marker gene analysis[1] (Extended Data Fig. 2b), many of these filtered barcodes are likely multiplets or nuclei contaminated with ambient mRNA.

All 75 reference cell types were present in the final filtered dataset of 144,438 nuclei (Fig. 1b; Extended Data Table 3) and expressed the expected marker genes[1] (Fig. 1d). Both neuronal and non-neuronal cell types showed high correlation with the corresponding reference cell types[1] (cosine similarity score > 0.83) and lower correlation to other subtypes within their class (Fig. 1e). This pattern was maintained when we considered either the paediatric or adult datasets on their own, with the majority of paediatric cell types showing only slightly lower similarity scores than the adults (Extended Data Table 3), which is likely due to the reference dataset only containing adult data. The cell composition of the samples was very similar with

121 no significant differences in cell type proportions between paediatric and adult samples or
122 between biological sexes (Fig. 1c; Extended Data Figure 2c-d; Extended Data Table 3). Similar
123 to the reference atlas[1], oligodendrocytes were the most common non-neuronal cell type and
124 Exc_L2-3_LINC00507_FREM3 was the most common neuronal subtype. Neuronal clusters had
125 a greater number of expressed genes and unique molecular identifiers (UMIs) compared to
126 non-neuronal cells (Extended Data Figure 3a), while excitatory neurons had a greater number
127 of genes detected per nucleus than inhibitory neurons (Extended Data Table 3). When
128 comparing the paediatric to adult cell types, there were no significant differences in the
129 number of genes or UMIs between the age categories. Overall, the quality and composition
130 of the paediatric and adult cell atlases were very similar.
131
132
133 **Spatial mapping of cell types reveals similar tissue cytoarchitecture in adult and paediatric**
134 **temporal cortex**
135
136 Next, we used spatial transcriptomics to explore the positions of our annotated cell types
137 within the temporal cortex. We generated Visium datasets from adult (31-year-old) and
138 paediatric (15-year-old) temporal cortex samples (two sections each; Extended Data Table 1;
139 Extended Data Fig. 4). The four Visium libraries were sequenced to a median depth of 87,178
140 reads per spot (median of 5,878 UMIs and 2,745 genes per spot) (Extended Data Table 4).
141
142 Using *cell2location*[26], we calculated cell type abundance estimates for each Visium spot, with
143 our annotated snRNA-seq dataset as a reference. Oligodendrocytes were the most common
144 cell type, while Exc_L2_LAMP5_LTK was the most abundant neuronal cell type (Extended Data
145 Fig. 5a). The annotated cell types mapped to their expected cortical layer locations across all
146 tissue sections (Fig. 2a; Extended Data Fig. 5b), matching the spatial expression of known
147 cortical layer marker genes[1,27,28] (Fig. 2b). These layered expression patterns were verified for
148 a subset of layer-specific marker genes using *in situ* hybridisation (Extended Data Fig. 6).

149 To examine the co-location of cell types within the layered structure of the temporal cortex,
150 non-negative matrix factorization (NMF) was performed resulting in 15 cellular
151 compartments, which were visualised across the Visium samples, revealing their spatial
152 distribution (Fig. 2c-d, Extended Data Fig. 5c). In both the paediatric and adult datasets, there
153 was clear co-location of the expected neuronal cell types within overlapping compartments
154 across the cortical layers. Layer 2 was dominated by Exc_L2_LAMP5_LTK (factor_11) and
155 Exc_L2-3_LINC00507_FREM (factor_5), layer 3 by Exc_L3-4_RORB_CARM1P1 (factor_13),
156 layer 4 by the *RORB* excitatory neuron subtypes (factor_12), layer 5 by the *THEMIS* excitatory
157 neuron subtypes (factor_10) and layer 6 by the *FEZF2* excitatory neuron subtypes (factor_14
158 and factor_1), with the latter extending into the white matter. Inhibitory neurons were
159 primarily associated with factors 6 and 2, which were more widely spread across the layers.
160 Interestingly, these factors were more strongly associated with layers 5/6 in the adult than in

161 the paediatric samples. The two astrocyte subtypes were confirmed to have distinct
162 distribution profiles, with Astro_L1-2_FGFR3_GFAP (factor_4) located primarily in layer 1 and
163 the white matter, and Astro_L1-6_FGFR3_SLC14A1 (factor_9) more widely distributed. The
164 remaining non-neuronal cell types were largely associated with factors located in layer 1 and
165 the white matter.

166 Overall, our spatial transcriptomic analyses provide support for our annotation approach,
167 showing the expected spatial distribution of annotated cell types, and revealing a largely
168 similar tissue cytoarchitecture in adult and paediatric temporal cortex tissue.

169

170 **A machine learning approach identifies new temporal cortex cell type markers**

171

172 To establish a standardized approach for defining cell types, it has been proposed to use the
173 minimum combination of gene markers that can classify a cell type and distinguish it from
174 other cell types[29,30]. Towards achieving this, Aevermann et al. (2021)[29] developed the machine
175 learning tool, *NS-Forest V2.0*, which they applied to the MTG cell atlas. Ideally, these MTG
176 minimal markers would be conserved in similar datasets to facilitate accurate comparisons
177 across different studies[31]. Indeed, we found that the majority of MTG cell atlas minimal
178 markers[29] (~94%) are expressed at significantly higher levels in the expected cell types than
179 in other cell types (Extended Data Fig. 7, Extended Data Table 5).

180

181 Application of the *NS-Forest V2.0*[29] algorithm to our down-sampled snRNA-seq datasets (see
182 Methods) revealed 202 paediatric and 196 adult minimal marker genes (Fig. 3; Extended Data
183 Table 5). The median F-beta score per cell type (the measure of the discriminative power of a
184 given combination of marker genes; paediatric=0.55; adult=0.6) and the average binary
185 expression score (a measure of an individual gene's classification power; paediatric=0.9;
186 adult=0.89) were comparable across age groups and only slightly lower than that obtained
187 for the MTG cell atlas (0.68 and 0.94 respectively)[29]. 47 paediatric (23.3%) and 45 adult
188 (23.0%) minimal markers overlapped with existing markers[29] (Fig. 3; Extended Data Table 5).
189 However, there was a greater overlap in minimal markers between the paediatric and adult
190 datasets, with 68 markers (~34%) present in both lists. MERFISH[32] spatial transcriptomic
191 analysis of a subset of minimal makers that were shared between paediatric and adult
192 datasets confirmed their co-expression with previously described minimal markers[29] in adult
193 (31-year-old) and paediatric (15-year-old) temporal cortex samples (Extended Data Fig. 8).

194

195 Our minimal marker analysis revealed improved markers for some cell types when compared
196 to the reference MTG cell atlas. In our datasets, the long non-coding RNA, *LINC01331*, is a
197 minimal marker for Exc_L2-3_LINC00507_FREM3 with a beta score of 1, indicating high
198 specificity. In contrast, one of the existing markers for this cell type, *PALMD*, is more highly
199 expressed in endothelial cells in our datasets (Fig. 3; Extended Data Fig. 9a-b). This

200 discrepancy is likely due to the lower percentage of endothelial cells in the MTG cell atlas
201 compared to our datasets (0.06% vs 0.9%)[1]. Similarly, one of the existing MTG cell atlas
202 markers for Exc_L5-6 _THEMIS_CRABP1, *OLFML2B*, is more highly expressed in other layer
203 5/6 neurons in our dataset, whereas our minimal marker, *POSTN*, shows greater specificity
204 (Fig. 3; Extended Data Fig. 9c-d). Additionally, UMAP analysis of our annotated datasets using
205 our minimal marker gene list for each age group, in comparison to an equivalent number of
206 random genes, resulted in better grouping of the cell subtypes into clusters, similar to the
207 original UMAP plot (compare Fig. 1a and Fig. 4 a-b). This analysis reveals that our shortlists of
208 ~200 marker genes capture much of the underlying transcriptomic diversity in our datasets.
209
210 Gene ontology (GO) analysis of our minimal marker gene lists revealed significant enrichment
211 of GO terms related to development, cell signalling, extracellular matrix and synapse
212 organisation, when considering the paediatric and adult datasets individually or together
213 (Extended Data Table 6). These results suggest that genes involved in neuronal development
214 and signalling are key to neuronal identity as the brain matures and in adult life. To further
215 assess the difference in cell type markers between our paediatric and adult datasets, we
216 expanded our analysis to include all genes with a high NS-Forest binary expression score (>
217 0.7)[29]. For most cell types, the majority of these top markers (>18 genes) were shared
218 between our paediatric and adult datasets (Fig. 4c; Extended Data Tables 7-8). The
219 oligodendrocytes showed the highest number of shared marker genes (53), as well as the
220 second highest number of paediatric-specific markers (22). Exc_L3-4_RORB_CARM1P1 had
221 the highest number of adult-specific marker genes (30), while Exc_L2-4_LINC00507_GLP2R
222 had no shared markers. GO analysis of the shared oligodendrocyte marker genes revealed
223 driver terms related to oligodendrocyte structure and function, including "structural
224 constituent of myelin sheath", while the top driver terms for the paediatric-specific markers
225 were "oligodendrocyte differentiation" and "myelination" (Extended Data Table 6). Overall,
226 our expanded marker gene analysis suggests that neuronal cell types show greater
227 dissimilarity between their paediatric and adult states than non-neuronal cells. It is likely that
228 more diversity in the non-neuronal marker gene profiles could be revealed with subdivision
229 into further subtypes.
230
231
232 **Differential gene expression analysis highlights enriched expression of genes associated**
233 **with neurodevelopment in paediatric samples.**
234
235 To identify genes that were upregulated in the paediatric cell populations and thus might be
236 involved in brain maturation, we conducted cell type-specific differential gene expression
237 analysis with *DESeq2*[33]. In total, we detected 165 significantly differentially expressed genes
238 (DEGs) across 21 cell types (123 upregulated in paediatric samples and 42 downregulated),
239 with some DEGs associated with multiple cell types (Fig. 5a; Extended Data Table 9-10). For
240 all DEGs, the change in expression was accompanied by a corresponding change in the

241 percentage of nuclei expressing the gene (Extended Data Table 10). *BayesSpace*[34] analysis of
242 a subset of DEGs in our Visium datasets confirmed that the genes were expressed at higher
243 levels in the 15-year-old compared to the 31-year-old (Extended Data Fig. 10).
244
245 Many of the excitatory neuron subtypes shared DEGs that are known to be developmentally
246 regulated in the mammalian brain (Fig. 5b-e,h). *LAMC3*, a subunit of the extracellular matrix
247 protein laminin, was upregulated in three paediatric subtypes (Exc_L3-5_RORB_ESR1, Exc_L2-
248 3_LINC00507_FREM3, Exc_L4-5_RORB_FOLH1B) (Fig. 5b-d,h). *LAMC3* plays a role in cortical
249 lamination in the mouse[35] and mutations are implicated in human brain heterotopias and
250 gyration defects[36,37]. Similarly, *S0X11*, a transcription factor that plays a role in embryonic and
251 adult neurogenesis in the mouse brain[38] and decreases in expression in the cerebral cortex
252 during development[39,40], was upregulated in paediatric Exc_L3-5_RORB_ESR1 and Exc_L2-
253 3_LINC00507_FREM3 (Fig. 5b-c,h). *FNBP1L* (*TOCA-1*) was upregulated in Exc_L2-
254 3_LINC00507_FREM3 and Exc_L2_LAMP5_LTK (Fig. 5c,e,h). FNBP1L promotes actin
255 polymerisation, regulating neurite outgrowth, and declines in expression over the course of
256 brain maturation in the rat[41]. Two genes, *STEAP2*, a metalloreductase, and the TNF receptor
257 *TNFRSF25* (*DR3*), were higher in adult Exc_L3-5_RORB_ESR1 and Exc_L4-5_RORB_FOLH1B
258 subtypes (Fig. 5b,d,h). *STEAP2* increases in expression during post-natal hippocampal
259 maturation in mice[42]. *TNFRSF25* is activated post-natally in the mouse brain, where it may
260 play a role in retention of motor control during aging[43]. These findings indicate that previously
261 reported expression dynamics for these genes in mammalian models are conserved in the
262 human temporal cortex. Importantly, our analysis reveals these patterns are specific to
263 groups of excitatory neuron subtypes.
264
265 The majority of the DEGs were not shared across the cell types. For example, *FGF13* (*FHF2*)
266 and *TENM1* were upregulated in paediatric Exc_L3-5_RORB_ESR1 (Fig. 5b). *FGF13* decreases
267 in expression with age in the mouse brain, where it regulates post-natal neurogenesis[44] and
268 axonal formation[45]. *TENM1* is a member of the teneurin transmembrane protein family that
269 regulates cytoskeletal organisation and neurite outgrowth, as well as shaping synaptic
270 connections[46-48]. *KCNG1,* a voltage gated-potassium channel (Kv6.1), was upregulated in
271 paediatric Exc_L2-3_LINC00507_FREM3 neurons (Fig. 5c), while *MYO16* (*MYR8*), an
272 unconventional myosin protein, was upregulated in the Exc_L2_LAMP5_LTK subtype (Fig. 5e).
273 Both of these genes decrease in expression with age in the mammalian brain[49,50].
274
275 In line with our minimal marker analyses, fewer genes were differentially expressed in non-
276 neuronal cells (Fig. 5f-g, Extended Data Table 10). In Astro_L1-6_FGFR3_SLC14A1, *PIK3R3* was
277 upregulated in paediatric samples, while *PFKFB2* was downregulated. *PIK3R3* is involved in
278 the PI3K-AKT growth signalling pathway, which is implicated in brain growth disorders[51].
279 *PFKFB2* is a bifunctional kinase/phosphatase that controls glycolysis. In contrast to our
280 findings, PFKFB2 expression is higher in juvenile rat hippocampal astrocytes than in adults,
281 where it may support energy demands during learning[52]. In oligodendrocytes, *NOTCH2* and

282 *RRAS2* were both upregulated in paediatric samples. *Notch2* expression decreases in the rat
283 cortex with age[53] and is proposed to regulate glial differentiation[54]. These results provide new
284 molecular candidates to expand our understanding of the mechanisms of astrocyte and
285 oligodendrocyte maturation.
286
287 To explore the trajectories of DEG expression, we employed *psupertime* pseudotime
288 trajectory analysis[55], focussing on the four excitatory neuron sub-types with the highest
289 number of DEGs. In support of our DESeq2 findings, several of the identified DEGs had non-
290 zero psupertime coefficients and therefore represent genes that are relevant to the ordering
291 of the cells in pseudotime[55] (Fig. 5i; Exc_L3-5_RORB_ESR1: 13/47 [28%], Exc_L2-
292 3_LINC00507_FREM3: 16/38 [42%], Exc_L4-5_RORB_FOLH1B 3/27 [11%] and
293 Exc_L2_LAMP5_LTK: 5/18 [28%]; Extended Data Table 11). When considering the pseudotime
294 trajectories for all DEGS in these excitatory neuron subtypes, the direction of the expression
295 matched the DESeq2 results (Supplementary Fig. 2-5). The pseudotime trajectories revealed
296 subtle expression dynamics within the analysed sample groups, showing that the majority of
297 DEGs gradually increase in expression with age from childhood to adolescence, followed by
298 a decrease in expression towards late adulthood.
299
300 Genes associated with intelligence quotient (IQ) and educational attainment (EA), as well as
301 those associated with accelerated evolution in humans, have recently been shown to be
302 enriched in adult temporal lobe cortical neurons, especially the Exc_L2-3_LINC00507_FREM3
303 subtype[56]. Since childhood is a key period of cognitive development[57], we explored whether
304 the same genes were found amongst our DEGs. Of the 149 DEGs found in at least one cell
305 type, 20 (13.42%, p=0.02) are known to be significantly associated with EA[58], 6 (4.02%, p=0.7)
306 with IQ[59] and 30 (20.13%, p=3.89E-07) with accelerated evolution in humans[60]. These
307 included several genes that are upregulated in paediatric samples, such as *MYO16*, *KCNG1*,
308 *FGF13* and *SOX11* (Extended Data Table 10).
309
310 Overall, we highlight several genes that are upregulated in children/adolescents which have
311 known roles in brain development and have been associated with cognitive ability. Our
312 analysis builds on previous knowledge by implicating specific cell subtypes and provides new
313 candidate genes that likely contribute to cell type-specific maturation processes.
314
315 **Gene pathways involved in cellular respiration and synaptic functioning are enriched in**
316 **paediatric cell types**
317
318 We next used gene set enrichment analysis (GSEA) to conduct a broad analysis of the gene
319 pathways that are differentially regulated across all brain cell types during brain maturation.
320 2,006 GOBP terms where enriched in the paediatric samples compared to the adults, while
321 866 were depleted (p<0.01 and q<0.1) (Extended Data Table 12). When focussing on the 25
322 most frequently enriched terms, the majority (10 terms) were associated with cellular

respiration pathways (Fig. 6; Extended Data Table 12). Six were associated with intra-cellular transport, including transport of neurotransmitters, while five were linked to neurotransmitter release and synaptic plasticity. Three terms, including the top enriched term, were associated with protein translation and modification. The majority of depleted terms (10 terms) were associated with synaptic processes (Fig. 6). A further six depleted terms were connected to neuronal morphogenesis, including axon and dendrite morphogenesis. Two of the top depleted terms were associated with axon ensheathment. Interestingly, neither of these terms were significantly enriched in oligodendrocytes or OPCs, while they were associated with neuronal sub types, and microglia.

Overall, our GSEA analysis points towards putative genetic pathways that may drive maturation in the paediatric brain. Cellular respiration processes needed to support the higher metabolic rates in the brain during childhood[61] may be enriched. Additionally, pathways related to strengthening synapses through neurotransmitter release may be enhanced. On the other hand, as synaptic pruning is underway[62], pathways that promote synaptic growth may need to be suppressed.

Cell type-specific expression of site-of-disease TBM biomarkers

The PCA aims to create reference atlases that can be used to improve our understanding of cell type-specific responses to disease in children[17]. Here, we used our snRNA-seq datasets to interrogate the cell type-specific expression of putative genetic biomarkers for TBM[23]. These biomarkers are enriched in the ventricular cerebrospinal fluid from children with TBM in comparison to controls with meningitis caused by other brain infections[23].

66 of the 76 TBM biomarkers were expressed in our dataset, with similar expression across the two age groups, and genes clearly clustering according to their relative expression across the broad cell type categories (Extended Data Fig. 11). The genes with the highest relative expression in our data were expressed by non-neuronal cell types, which is in line with the view that immunological activity of supporting cells and their intercellular signalling interactions are important drivers of the immune response to TBM[63]. Several of these biomarkers (e.g. *FADS2*, *AMOT* and *ALDH6A1*) were enriched in the two astrocyte subtypes, potentially pointing towards a prominent role for astrocytes in the host response to TBM.

Our analyses also clearly revealed subsets of biomarkers that are more highly expressed by neuronal subtypes than non-neuronal cell types. This included biomarkers that were associated with Exc_L2_LAMP5_LTK, Exc_L2-4_LINC00507_GLP2R and Exc_L5-6_THEMIS_C1QL3 (*LYNX1*, *FAIM2*, *MAP1A*, *TUBB4A*). This is line with the finding that neuronal excitotoxicity is elevated in TBM[23] and suggests that specific excitatory neuron subtypes may be contributing to this signal.

364 Interestingly, the two most enriched genes in the TBM biomarker dataset, *CXCL9* and *CXCL11*,
365 were either completely absent from our datasets (*CXCL11*) or expressed by very few nuclei
366 (*CXCL9*). The absence of these interferon-inducible chemokines in our datasets from
367 uninfected tissue, supports the proposition that they are indeed biomarkers from the site-of-
368 disease[64] in both adults and children with TBM, and could also reflect the contribution of
369 peripheral immune cells recruited to the brain during infection.
370
371
372 **Discussion**
373
374 The brain is the most complex organ in the human body, which continuously changes as we
375 mature. Here, we begin to unmask the molecular mechanisms guiding these processes in the
376 temporal cortex, using single cell and spatial transcriptomics to compare similar cell types
377 between paediatric and adult datasets.
378
379 To facilitate accurate comparisons of cell types across age groups, we used the existing Allen
380 Brain Map MTG cell atlas[1] to annotate our datasets. This demonstrated that the reference
381 atlas, generated from adult snRNA-seq datasets, is indeed generalisable[31], and can be used
382 to classify cell types from samples of different ages. This generalisability is essential for
383 healthy human reference atlases to serve as a baseline to improve our understanding of
384 human development and disease[3]. Our samples and those in the reference MTG cell atlas
385 include neurosurgical tissue from donors with epilepsy, and while the analysed tissue is not
386 from the site of pathology, it is important to view our findings in light of the patient diagnosis.
387 Previous research comparing gene expression between the neurosurgical and post-mortem
388 samples used in the reference MTG cell atlas found a strong correlation of expression
389 between cell types across conditions[1]. In addition, a comparison of samples from 45 adult
390 donors with epilepsy to the post-mortem samples from the reference MTG cell atlas found a
391 similar number of genes and similar cell abundance per cell subclass across tissue sources,
392 however they did find more variation for these parameters in neurosurgical samples[65]. As
393 more paediatric MTG samples of post-mortem and neurosurgical origin become available, it
394 will be important to conduct similar analyses to determine if these findings hold for the
395 paediatric temporal cortex.
396
397 Our machine-learning marker gene analysis shows that while the cell type classifications,
398 which are based on the expression of thousands of genes, can be transferred onto new
399 datasets, the minimal markers that define the cell types do vary across datasets. Only a
400 quarter of our *NS-Forest* minimal markers overlap with the existing MTG cell atlas minimal
401 markers[29]. The differences in the single cell transcriptomics technologies used to generate
402 our dataset and the MTG cell atlas may account for much of this discrepancy. Nonetheless,
403 our analyses suggest that some of our markers may provide better discrimination between
404 cell types than existing markers. These results highlight a challenge that the HCA faces to

revise cell type markers as more datasets are made available to ensure that the cell type classification is as widely applicable as possible.

Similar to analyses of aging in the mouse[66], our analyses show there is little change in cell type composition within the temporal cortex during human brain maturation. However, our differential expression analysis highlights differences in cell states between specific paediatric and adult cell subtypes. Recently, the supragranular excitatory pyramidal neurons in the MTG have been shown to have high transcriptional diversity[1,67], large arborisations[68] and electrophysiological properties that impact signal integration and encoding[69-72] in ways that may contribute to cognition. Since cognitive ability is a key feature that is established during childhood[68], our analysis offers an opportunity to explore how cell type-specific gene expression dynamics contribute to cognitive development. Interestingly, two of the 21 highlighted cell types were the layer 2/3 excitatory neurons, Exc_L2_LAMP5_LTK and Exc_L2-3_LINC00507_FREM3, that have recently been associated with human cognition[56]. In line with these findings, several of the DEGS associated with these cell types, including *FNBP1L*[73] and *SOX11*[74], have been implicated in cognitive ability and intelligence. Overall, our data points towards genes that may play roles in cognitive development specifically within these excitatory neurons.

The relatively low number of genes implicated in our differential expression analysis in comparison to similar studies in mouse[66] suggests that the difference between the paediatric and adult brain are subtle. However, the inherent high variability in human gene expression data may mask some of the differential gene expression in our limited sample. Nonetheless, our pseudotime trajectory analyses reveals some of the expression dynamics that may be occurring during childhood, with many genes rising in expression towards adolescence and dropping off in adulthood. As the HCA database for the human temporal cortex expands, it will be important to build on these analyses with more samples. Binning of samples of similar age will provide a higher resolution analysis of cell type-specific gene expression trajectories over the course of brain maturation.

Finally, we have provided the first single nucleus gene expression datasets for the brain that includes data from black Southern African donors, thus increasing the diversity of the HCA database. We demonstrate how this resource can be used to deconvolute site-of-disease biomarker analyses for TBM, pinpointing which cell types may be driving altered gene expression profiles in the brain. Importantly, these investigations have the potential to contribute to the development of effective treatments, that are tailored to specific needs of both adult and paediatric patients.

Methods

446 **Human samples**
447 Ethical approval was granted for the collection and use of paediatric and adult human brain
448 tissue by the University of Cape Town Human Research Ethics Committee (UCT HREC REF
449 016/2018; sub-studies 146/2022 and 147/2022). The human brain tissue samples used to
450 generate new datasets were obtained by informed consent for studies during temporal lobe
451 surgical resections to treat epilepsy and/or cancer performed at the Red Cross War Memorial
452 Children's Hospital and Constantiaberg Mediclinic in Cape Town, South Africa. The samples
453 used in this study were of temporal cortex origin and represent radiologically
454 and macroscopically normal neocortex within the pathological context (details in Extended
455 Data Table 1). Race was recorded by the clinical teams based on their knowledge of the
456 donors. The category "black South African" includes both black and mixed race ancestries.
457 Upon resection, samples were placed in carbogenated ice-cold artificial cerebral spinal fluid
458 (aCSF) containing in (mM): 110 choline chloride, 26 $NaHCO_3$, 10 D-glucose, 11.6 sodium
459 ascorbate, 7 $MgCl_2$, 3.1 sodium pyruvate, 2.5 KCl, 1.25 NaH_2PO_4, and 0.5 $CaCl_2$ (300 mOsm)
460 and immediately transported to the laboratory (~20 minutes). Tissue blocks containing the
461 full span from pia to white matter were prepared and either flash frozen in liquid nitrogen or
462 embedded in optimal cutting temperature compound (OCT) and stored at -80°C. The OCT-
463 embedded samples were flash frozen in a 10×10 mm^2 cryomold which was either frozen
464 directly in liquid nitrogen or placed in a container of isopentane (Merck) which was in turn
465 placed in liquid nitrogen at the same level as the isopentane. The publicly available snRNA-
466 seq datasets[24]**,** generated from samples obtained during elective surgeries performed at
467 Universitair Ziekenhuis Leuven, Belgium, were downloaded from the Sequence Read Archive
468 database.
469
470 **Nuclei isolation for snRNA-seq**
471 Nuclei were isolated according to a protocol adapted from Habib et al. (2017)[75] and the 10X
472 Genomics nuclei isolation protocol (CG000124, User Guide Rev E). Frozen brain tissue was
473 homogenised in a dounce-homogeniser containing 2 ml ice-cold lysis solution (Nuclei EZ Lysis
474 Buffer [Sigma-Aldrich, NUC101] or Nuclei PURE Lysis buffer [Sigma-Aldrich, NUC201] with 1
475 mM dithiothreitol [DTT, Promega, P1171, US] and 0.1% Triton X-100 [Sigma-Aldrich, NUC201-
476 1KT, US]). Homogenisation was done 20 times with the loose pestle A followed by 20 times
477 with the tight pestle B. An additional 2 ml lysis solution was added, and the sample was
478 incubated for 5 minutes on ice. The sample was centrifuged at 500 x g for 5 minutes at 4°C
479 after which the supernatant was discarded and the nuclei resuspended in 3 ml ice cold nuclei
480 suspension buffer (1x phosphate-buffered saline [PBS, Sigma-Aldrich, P4417-50TAB, US]),
481 0.01% bovine serum albumin [BSA, Sigma-Aldrich, A2153-10G, US], and 0.2 U/µl RNAsin Plus
482 RNase inhibitor [Promega, N2615, US]). Resuspended nuclei were passed through a 40 µm
483 filter and centrifuged at 900 x g for 10 minutes at 4°C. The supernatant was discarded and
484 pelleted nuclei were resuspended in 3 ml blocking buffer (1xPBS [Sigma-Aldrich, P4417-
485 50TAB, US], 1% BSA [Sigma-Aldrich, A2153-10G, US], 0.2 U/µl RNAsin Plus RNase inhibitor
486 [Promega, N2615, US]).

487

488 To remove myelin debris, 30 µl of myelin removal beads [Miltenyi Biotec. 130-096-733, US]
489 was added to the solution which was mixed by gently pipetting 5 times. The sample was
490 incubated for 15 minutes at 4°C after which it was mixed with 3 ml blocking buffer and
491 centrifuged at 300 x g for 5 minutes at 4°C. The supernatant was removed and the nuclei were
492 resuspended in 2 ml clean blocking buffer. The sample was transferred to a 2 ml tube and
493 placed on a Dynamag magnet for 15 minutes at 4°C. The supernatant was transferred to a
494 new tube and stored on ice. An aliquot of trypan blue stained nuclei was counted using a
495 haemocytometer to determine the nuclei concentration and the volume to use in snRNA-seq
496 library preparation.

497

498 **10X Genomics snRNA-seq library preparation**

499 snRNA-seq library preparation was carried out using the 10x Genomics Chromium Next Gem
500 Single Cell 3' Reagent Kit (v3.1) according to manufacturer's protocols (CG000204, User Guide
501 Rev D), targeting 10,000 nuclei per sample. At step 2.2d and 3.5e, the libraries were amplified
502 using 11 cycles and 13 cycles, respectively. Library quality and concentration was assessed
503 using either the TapeStation or Bioanalyser (Agilent) and Qubit (Invitrogen) at the Central
504 Analytical Facility (CAF, University of Stellenbosch). cDNA libraries were sequenced by
505 Novogene (Singapore) on either the Illumina HiSeq or NovaSeq system using the Illumina High
506 Output kits (150 cycles).

507

508 **snRNA-seq read alignment and gene expression quantification**

509 Fastq files were aligned to the human reference transcriptome (GRCh38) and quantified using
510 the count function from the 10X Genomics Cell Ranger v6.1.1 software (Cell Ranger, RRID
511 SCR_017344) (Code availability: script 1). The inclusion of introns was specified in the count
512 function. An automatic filtering process was performed to remove barcodes corresponding
513 to background noise which have very low UMI counts.

514

515 **snRNA-seq quality control**

516 The resulting count matrices were processed using a pipeline adapted from the Harvard Chan
517 Bioinformatics Core (https://hbctraining.github.io/scRNA-seq_online/). The filtered gene
518 barcode matrix for each sample was imported into R (V.4.2.0) using the Read10X function
519 from the Seurat (v.2.0)[25]. Nuclei-level filtering was performed to remove poor quality nuclei
520 according to their number of UMIs (nUMIs) detected, number of genes detected (nGene),
521 number of genes detected per UMI (log10GenesPerUMI), and the fraction of mitochondrial
522 read counts to total read counts (mitoRatio) (Code availability: script 2). Nuclei that met the
523 following criteria were retained: nUMI > 500, nGene > 250, log10GenesPerUMI > 0.8 and
524 mitoRatio < 0.2. Gene-level filtering was performed to remove genes that had zero counts in
525 all nuclei, remove genes expressed in fewer than 10 nuclei, and remove mitochondrial genes
526 from the gene by cell counts matrix. Three doublet removal tools namely

527 DoubletFinder[76](Code availability: script 3), DoubletDecon[77] (Code availability: script 4), and
528 Scrublet[77] (Code availability: script 5,6) were used to identify doublets for each dataset
529 individually. The sample-specific parameters of each of the tools were adjusted according to
530 the specified guidelines. To achieve a balance between the false positive and false negative
531 rate of the different doublet detection tools, all doublets identified by DoubletFinder as well
532 as the intersection of the doublets identified by DoubletDecon and Scrublet, were removed[77].
533

534 **snRNA-seq data normalization, integration and clustering**

535 Principal component analysis was performed to evaluate known sources of within-sample
536 variation between nuclei, namely the mitoRatio and cell cycle phase (Code availability: script
537 7). The UMI counts of the 3000 most variable features were normalised and scaled on a per
538 sample basis by applying Seurat's SCTransform function with mitoRatio regressed out. A
539 Uniform Manifold Approximation and Projection (UMAP) analysis was performed on the
540 merged object to assess whether integration was necessary. The datasets were subsequently
541 integrated using Seurat's SelectIntegrationFeatures, PrepSCTIntegration,
542 FindIntegrationAnchors, and IntegrateData functions (Code availability: script 7). To cluster
543 the datasets following integration, dimensionality reduction was first performed using UMAP
544 embedding, specifying 40 dimensions (Code availability: script 8). The Seurat FindClusters
545 function was then applied at a resolution of 0.8.
546

547 **snRNA-seq cluster annotation**

548 Two levels of annotation were performed. Clusters were initially annotated as one of the
549 major brain cell types (level 1 annotation) based on the expression of known markers genes
550 (Code availability: script 9). Label transfer was then performed using Seurat's TransferData
551 function with Allen Brain Map MTG atlas[1] as a reference dataset (level 2 annotation) (Code
552 availability: scripts 10-11). This resulted in each barcode in the query dataset receiving a
553 predicted annotation based on a similarity score to an annotated cell type in the reference.
554 Barcodes were then filtered to remove those with discordant level 1 and level 2 annotations
555 (e.g. barcodes with "oligodendrocyte" level 1 annotation and "Exc_L4-5_RORB_FOLH1" level
556 2 annotation) (Code availability: script 12). To validate the annotation, the expression of
557 known marker genes was assessed. Cosine similarity scores were computed to compare the
558 transcriptomic similarity of each of the annotated query cell types to the 75 reference MTG
559 cell types using the SCP package (https://github.com/zhanghao-njmu/SCP) (Code availability:
560 script 13). This was achieved by computing cosine similarity scores for each pair of query and
561 reference cell types using the expression of the top 2000 shared highly variable features
562 between the query and reference datasets. The log normalised expression counts were used
563 for this purpose (RNA assay, data slot). To assess the difference between the paediatric and
564 adult datasets relative to the reference, the above cosine similarity analysis was repeated on
565 the paediatric and adult datasets individually (Code availability: script 13).
566

567 **NS-Forest machine learning marker analysis of snRNA-seq datasets**
568 The NS-Forest tool (v2.0)[29,30] was used to identify combinations of marker genes uniquely
569 defining each annotated cell type (Code availability: script 14-15) in the paediatric and adult
570 datasets separately. The number of nuclei per sample was randomly down-sampled to that
571 of the sample with the fewest nuclei (n=4,865). A random-forest model was used to select a
572 maximum of 15 marker genes per cell type based on them being both highly expressed as
573 well as uniquely expressed within a cell type compared to other cell types (i.e., the top Gini
574 Index ranked features with positive expression values). The number of trees chosen for this
575 model was 30,000, the cluster median expression threshold was set to the default value of
576 zero, the number of genes used to rank permutations of genes by their F-beta-score was 6,
577 and the beta weight of the F score was set to 0.5. The aforementioned parameters were set
578 according to the parameters described in Aevermann et al. (2021)[29], allowing the outputs to
579 be directly compared to their markers and to the Allen Brain Map MTG atlas minimal
580 markers[1]. To assess the relevance of these markers in terms of their capacity to distinguish
581 different cell types in a UMAP analysis, the SCT and integration methods were repeated using
582 either a random set of genes or the NS-Forest markers as anchors[29] (Code availability: script
583 16).
584
585
586 **DESeq2 age-dependent differential gene expression analysis of snRNA-seq datasets**
587 DESeq2[33] was used to identify genes that were differentially expressed with age (Code
588 availability: script 17). The unnormalized counts were aggregated across all nuclei for each
589 cluster and sample to generate a 'pseudobulk' counts matrix with the counts from technical
590 replicates collapsed to the level of biological replicates. Genes were filtered to only include
591 those expressed in more than 10% of nuclei for a given cell type. Principal component analysis
592 was performed on each cell type separately in order to assess the variation between samples
593 and determine which variables were contributing most to inter-sample variation from a set
594 of possible variables. The collapsed counts served as input into DESeq2's
595 DESeqDataSetFromMatrix function in which the design formula ~single_cell_chemistry +
596 age_group was specified to treat the age_group (paediatric vs adult) as the variable of interest
597 while the effect of single_cell_chemistry (version2 vs version3 chemistry) was regressed out.
598 A hypothesis test was performed using the Wald test. The null hypothesis for each gene was
599 that there is no difference in gene expression between the sample groups (i.e Log2Fold
600 Change = 0). A Wald test statistic was determined for each gene together with the associated
601 p-value after which the p-values were adjusted for multiple testing using the Benjamini-
602 Hochberg method. Positive log2 Fold Changes represent genes which are upregulated in
603 paediatric samples compared to adult samples (p_{adj} <0.05).
604
605 **Pseudotime trajectory analysis with psupertime**
606

607 To validate the differentially expressed genes identified with DESeq2, a pseudotime trajectory
608 analysis was performed for a subset of excitatory neuron subtypes using the psupertime
609 package[55] (Code availability: script 18). Psupertime is a supervised approach that uses time-
610 series labels as input to improve the identification of time-varying genes. Each cell type of
611 interest (Exc L3-5 RORB ESR1, Exc L2 LAMP5 LTK, Exc L4-5 RORB FOLH1B, Exc L2-3 LINC00507
612 FREM3) was individually sub-setted from the Seurat object after which a single cell
613 experiment (sce) object was generated using the log normalized counts (RNA assay, data slot).
614 The donor age (4, 5, 7, 9, 15, 20, 24, 26, 31, 41, 50) was included as metadata in the object.
615 The psupertime function was applied to the sce object with the sel_genes argument
616 specifying all genes to be used. An automatic filtering step was performed to remove genes
617 expressed in fewer than 10% of cells for each cell type. As an output of the function, the beta
618 coefficients for the association of each gene with pseudotime were extracted and plots were
619 generated showing the expression trajectories of the DESeq2 DEGs with pseudotime.
620 Additionally, the overlap between the DESeq2 DEGs and genes changing as a function of
621 pseudotime (Psupertime-relevant genes) was determined.
622
623 **Pathway enrichment analysis of snRNA-seq datasets**
624 GO analysis of NS-Forest marker genes was performed on the gProfiler web server[78] using
625 default settings (p_{adj} <0.05) with "highlight diver terms in GO" selected.
626
627 DEGs identified by DESeq2 (see Extended Data Table 10) that were associated with EA and IQ,
628 as well as those associated with accelerated evolution in humans (HARs), were determined
629 by comparing the list of neuronal DEGS to the EA, IQ and HAR gene lists used by Driessens et
630 al. (2023)[56], which were subsets of the lists from Lee et al. (2018)[58], Savage et al. (2018)[59] and
631 Doan et al. (2016)[60] respectively. A hypergeometric test was performed to test the
632 significance of the results relative to chance (Code availability: script 19).
633
634 GSEA on the DESeq2 output for all genes was performed using the Broad Institute's GSEA
635 software (https://www.gsea-msigdb.org/gsea/msigdb) (Code availability: script 20). GSEA
636 aggregates the information from many genes to identify enriched functional pathways,
637 allowing us to interrogate the gene signature changes across all cell types, including those
638 that did not show any significant DEGs[66]. The gene lists for each cell type were queried against
639 the C5 GO Biological Processes collection comprising of gene sets derived from the GO
640 Biological Process ontology. The input lists of genes were ranked according to the -log(p-
641 value)*$\log_2$FoldChange for each gene. The parameters specified to the GSEA function
642 included number of permutations (nperm)=1000, minimum gene set size (set_min=15),
643 maximum gene set size (set_max=200), excludes genes that have no gene symbols (collapse)=
644 No_Collapse, value to use for the single identifier that will represent all identifiers for the
645 gene (mode)=Max_probe, normalised enrichment score method (norm)= meandiv, weighted
646 scoring scheme (scoring_scheme) = classic. Positive Normalised Enrichment Scores (NES)
647 represent genes that were upregulated in the paediatric population compared to the adult

648 population ($p<0.01$ and $q<0.1$). To visualise the output of universally enriched pathways
649 across multiple cell types, the top 25 most frequently appearing positively and negatively
650 associated terms were plotted. Additionally, for five cell types of interest [which had DEGs
651 meeting the threshold of $p<0.05$ and abs($\log_2$FC)>0.1], the top 5 positively associated terms
652 were plotted.
653
654 **Analysis of site-of-disease TBM markers**
655
656 The dittoheatmap function from the dittoSeq package[79] was used to generate heatmaps for
657 the expression of the TBM biomarkers (upregulated genes listed in Rohlwink et al. 2019,
658 Supplementary Table 5[23]) across cell types in the paediatric and adult datasets individually.
659 Additionally, Seurat's dotplot function[25] was used to visualize the level of expression and
660 proportion of nuclei expressing the markers across cell types (Code availability: script 21).
661 Prior to generating the plots, the TBM marker genes were filtered to remove those expressed
662 in 15 nuclei or fewer across all cell types. Gene counts for each marker were aggregated
663 across cell types and scaled. The markers were clustered according to their expression profiles
664 using dittoheatmap's default hierarchical clustering method (Euclidean, complete). The
665 clustering order and dendrogram from this output for the peaditaric datasets were used to
666 generate dotplots for both peaditaric and adult datasets (Code availability: script 21).
667
668 **snRNA-seq data plots**
669 Plots were produced with Seurat[25], ggplot2[80], ShinyCell[81] and Microsoft Excel.
670
671 **10x Genomics Visium library preparation**
672 Frozen OCT embedded temporal cortex tissue samples were scored using a pre-chilled razor
673 blade to fit in the Spatial Gene Expression slide capture areas. 10 µm-thick sections were cut
674 using a cryostat (Leica CM1860/CM1950) and collected onto the Spatial Gene Expression slide
675 capture areas. Two replicate sections of the 15-year-old (10 µm apart) and two replicate
676 sections of 31-year-old (40 µm apart) were collected. The spatial Gene Expression slides with
677 tissue sections were stored in a sealed container at -80°C. Captured sections were
678 Haematoxylin and Eosin (H&E) stained according to the 10x Genomics Demonstrated Protocol
679 Guide (CG000160, Rev B). Brightfield images of the stained sections were captured using an
680 EVOS M5000 microscope (Thermo Fisher Scientific) at 20x magnification without
681 coverslipping. Overlapping images of the sections including the fiducial frame were stitched
682 together using Image Composite Editor-2.0.3 (Microsoft). Visium libraries were prepared
683 from the stained tissue sections following the Visium Spatial Gene Expression Reagents Kit
684 User Guide (CG000239, Rev D). At Step 1.1 the tissue was permeabilised for 12 minutes as
685 determined using the Visium Spatial Gene Expression Tissue Optimisation User Guide
686 (CG000238, Rev D). At Step 3.2, cDNA was amplified using 20 cycles. Library quality and
687 concentration was assessed using TapeStation (Agilent) and Qubit (Invitrogen) at the Central

688 Analytical Facility (CAF, University of Stellenbosch). Libraries were sequenced by Novogene
689 (Singapore) on the Illumina NovaSeq system using the Illumina High Output kits (150 cycles).
690

691 **Visium read alignment and gene expression quantification**

692 The H&E images were processed using the 10X Genomics Loupe Browser V4.0 Visium Manual
693 Alignment Wizard. 10X Genomics Space Ranger *count* (10X Space Ranger V1.3.0) was used to
694 perform alignment of FASTQ files to the human reference transcriptome (GRCh38), tissue
695 detection, fiducial detection and barcode/UMI counting.
696

697 **cell2location analysis of Visium datasets**

698 The average number of nuclei per Visium spot was determined using Vistoseg[82] (Code
699 availability: script 22). Cell2location (version 0.7a0)[26] was used to spatially map the brain cell
700 types by integrating the Visium data count matrices (Space Ranger output) with the
701 annotated snRNAseq datasets (Code availability: script 23). To avoid mapping artifacts,
702 mitochondrial genes were removed from the Visium datasets prior to spatial mapping.
703 Reference signatures of the 75 annotated cell populations were derived using a negative
704 binomial regression model using the default values (Code availability: script 24).
705 Unnormalized and untransformed snRNA-seq mRNA counts were used as input in the
706 regression model for estimating the reference signatures (Code availability: script 24. The
707 snRNA-seq mRNA counts were filtered to 14,209 genes and 144,438 cells. The cell2location
708 model for estimating the spatial abundance of cell populations was filtered to 14,197 genes
709 and 14,324 cells that were shared in both the snRNA-seq and Visium data. The following
710 cell2location parameters were used: training iterations = 30,000 cell per location, N^ = 7
711 (estimated using Vistoseg segmentation results), Normalization (ys) alpha prior = 20 (Code
712 availability: script 25). To visualise the cell abundance in spatial coordinates 5 % quantile of
713 the posterior distribution was used, which represents the value of cell abundance that the
714 model has high confidence in (Code availability: script 26). Cell2location's Non-negative
715 Matrix Factorization (NMF) was used to identify cellular compartments and cell types that co-
716 locate from the cell type abundance estimates. NMF was tested using a range of factors (5 to
717 30) for the "n_fact" parameter (Code availability: script 26). n_fact=15 was chosen as it clearly
718 grouped the oligodendrocyte, astrocyte and excitatory neuron cell sub-types into known
719 tissue zones i.e. the layers of the cortex (Code availability: script 27).
720

721 **BayesSpace analysis of Visium datasets**

722 The raw gene expression counts from Space Ranger were normalized, log transformed and
723 principal component analysis was performed on the top 2000 highly variable genes. To obtain
724 high-resolution gene expression for selected genes, the principal component values were
725 mapped back to their original log-transformed gene expression space (spot level) using the
726 default BayesSpace[34] regression (Code availability: script 28). To do this the principal
727 components from the original data were used as predictors in training the model for each
728 gene, in which the results were the measured gene expression at the spot level. The trained

729 model was then used to predict the gene expression at sub spot level using high resolution
730 PCs. The high-resolution model was trained using default values except for the following
731 parameters: 7 PCs, Number of clusters = 8, nrep = 100,000, burn-in = 10,000. The BayesSpace
732 outputs for each sample were quantified for spots with expression level > 0 and displayed as
733 boxplots (Code availability: script 29).
734
735 ***In situ* Hybridisation Chain Reaction (HCR) on frozen human tissue sections**
736 10 µm thick frozen sections were collected on Histobond+ slides (Marienfeld) and stored at -
737 20°C. The *In situ* HCR protocol was carried out on tissue sections as detailed in Choi et al.
738 (2016)[83] using reagents, probes and hairpins purchased from Molecular Instruments. Probes
739 were ordered for the following genes: *RELN* (NM_005045.4), *FABP7* (CR457057.1), *AQP4*
740 (NM_001650.5), *RORB* (NM_006914.4), *CLSTN2* (NM_022131.3) and *TSHZ2* (NM_173485.6).
741 When necessary to quench lipofuscin autofluorescence, sections were rinsed after HCR in 1x
742 PBS and treated with 200 µl TrueBlack (Biotium) for 30 sec. Slides were rinsed in PBS, stained
743 with Hoescht (Thermofisher) and mounted using SlowFade Gold Antifade Reagent
744 (Invitrogen). Sections were imaged using the LSM 880 Airyscan confocal microscope (Carl
745 Zeiss, ZEN SP 2 software) using the 40X or 60X objective.
746
747 **MERFISH analysis on frozen temporal cortex tissue sections**

748 10 µm thick frozen sections were cut from frozen OCT embedded temporal cortex tissue
749 samples using a cryostat (Leica CM1950). Sections from a peaditaric and adult sample were
750 collected onto the same MERSCOPE coverslip (VIZGEN 2040003), fixed and stored in 70%
751 ethanol following the instructions in the VIZGEN protocol (Fresh & Fixed Frozen Tissue
752 Sectioning & Shipping Procedure Rev A, Doc. number 91600107). The slide was processed on
753 the VIZGEN MERSCOPE system by the MRC Weatherall Institute of Molecular Medicine Single
754 Cell Facility (University of Oxford) within 1 month of storage. Sections were photobleached
755 for 10 hours at 4°C and then washed in 5 ml Sample Prep Wash Buffer (VIZGEN 20300001) in
756 a 5 cm petri dish. Sections were incubated in 5 ml Formamide Wash Buffer (VIZGEN
757 20300002) at 37°C for 30 min and hybridized at 37°C for 36 to 48 hours by using 50 µl of
758 VIZGEN-supplied custom Gene Panel Mix according to the manufacturer's instructions.
759 Following hybridization, sections were washed twice in 5 ml Formamide Wash Buffer for 30
760 min at 47°C. Sections were then embedded in acrylamide by polymerizing VIZGEN Embedding
761 Premix (VIZGEN 20300004) according to the manufacturer's instructions. Following
762 embedding, sections were digested in Digestion Pre-Mix (VIZGEN 20300005) and RNase
763 inhibitor (New England Biolabs M0314L) for 3 h at 37°C and then cleared for 16 to 24 hours
764 with a mixture of VIZGEN Clearing Solution (VIZGEN 20300003) and Proteinase K (New
765 England Biolabs P8107S) according to the Manufacturer's instructions. Following clearing,
766 sections were washed twice for 5 min in Sample Prep Wash Buffer (PN 20300001) and then
767 stained with VIZGEN DAPI and PolyT Stain (PN 20300021) for 15 min followed by a 10 min
768 wash in Formamide Wash Buffer. Formamide Wash Buffer was removed and sections were

769 washed with Sample Prep Wash Buffer during MERSCOPE imaging set up. A mixture of 100
770 ml of RNAse Inhibitor (New England BioLabs M0314L) and 250 ml of Imaging Buffer Activator
771 (PN 203000015) was added to the cartridge activation port to a prethawed and mixed
772 MERSCOPE Imaging cartridge (VIZGEN PN1040004). 15 ml mineral oil (Millipore-Sigma
773 m5904-6X500ML) was added on top of the activation port and the MERSCOPE fluidics system
774 was primed according to VIZGEN instructions. The flow chamber was assembled with the
775 section coverslip according to VIZGEN specifications and the imaging session was initiated
776 after collection of a 10X mosaic DAPI image and selection of the 1cm^2 imaging area. MERFISH
777 data was visualised using the VIZGEN MERSCOPE Vizualizer software (version 2.3.3330.0).

778

779 **References**

780

781 1 Hodge, R. D. *et al.* Conserved cell types with divergent features in human versus
782 mouse cortex. *Nature* **573**, 61-68 (2019).
783 2 Bakken, T. E. *et al.* Comparative cellular analysis of motor cortex in human, marmoset
784 and mouse. *Nature* **598**, 111-119, doi:10.1038/s41586-021-03465-8 (2021).
785 3 Regev, A. *et al.* The Human Cell Atlas. *Elife* **6**, doi:10.7554/eLife.27041 (2017).
786 4 Network, B. I. C. C. A multimodal cell census and atlas of the mammalian primary
787 motor cortex. *Nature* **598**, 86-102, doi:10.1038/s41586-021-03950-0 (2021).
788 5 Darmanis, S. *et al.* A survey of human brain transcriptome diversity at the single cell
789 level. *Proc Natl Acad Sci U S A* **112**, 7285-7290, doi:10.1073/pnas.1507125112 (2015).
790 6 Li, M. *et al.* Integrative functional genomic analysis of human brain development and
791 neuropsychiatric risks. *Science* **362**, doi:10.1126/science.aat7615 (2018).
792 7 Velmeshev, D. *et al.* Single-cell analysis of prenatal and postnatal human cortical
793 development. *Science* **382**, eadf0834, doi:10.1126/science.adf0834 (2023).
794 8 Werling, D. M. *et al.* Whole-Genome and RNA Sequencing Reveal Variation and
795 Transcriptomic Coordination in the Developing Human Prefrontal Cortex. *Cell Rep* **31**,
796 107489, doi:10.1016/j.celrep.2020.03.053 (2020).
797 9 Kang, H. J. *et al.* Spatio-temporal transcriptome of the human brain. *Nature* **478**, 483-
798 489, doi:10.1038/nature10523 (2011).
799 10 Colantuoni, C. *et al.* Temporal dynamics and genetic control of transcription in the
800 human prefrontal cortex. *Nature* **478**, 519-523, doi:10.1038/nature10524 (2011).
801 11 Donertas, H. M. *et al.* Gene expression reversal toward pre-adult levels in the aging
802 human brain and age-related loss of cellular identity. *Sci Rep* **7**, 5894,
803 doi:10.1038/s41598-017-05927-4 (2017).
804 12 Bourgeois, J. P. & Rakic, P. Changes of synaptic density in the primary visual cortex of
805 the macaque monkey from fetal to adult stage. *J. Neurosci.* **13**, 2801-2820,
806 doi:10.1523/JNEUROSCI.13-07-02801.1993 (1993).
807 13 Huttenlocher, P. R. & Dabholkar, A. S. Regional differences in synaptogenesis in human
808 cerebral cortex. *J. Comp. Neurol.* **387**, 167-178, doi:10.1002/(sici)1096-
809 9861(19971020)387:2<167::aid-cne1>3.0.co;2-z (1997).
810 14 Petanjek, Z. *et al.* Extraordinary neoteny of synaptic spines in the human prefrontal
811 cortex. *Proc Natl Acad Sci U S A* **108**, 13281-13286, doi:10.1073/pnas.1105108108
812 (2011).

15 Paus, T., Keshavan, M. & Giedd, J. N. Why do many psychiatric disorders emerge during adolescence? *Nature Reviews Neuroscience* **9**, 947-957, doi:10.1038/nrn2513 (2008).

16 Jaffe, A. E. *et al.* Developmental and genetic regulation of the human cortex transcriptome illuminate schizophrenia pathogenesis. *Nat. Neurosci.* **21**, 1117-1125, doi:10.1038/s41593-018-0197-y (2018).

17 Taylor, D. M. *et al.* The pediatric cell atlas: defining the growth phase of human development at single-cell resolution. *Dev. Cell* **49**, 10-29 (2019).

18 Tishkoff, S. A. *et al.* The genetic structure and history of Africans and African Americans. *Science* **324**, 1035-1044, doi:10.1126/science.1172257 (2009).

19 PRB. *World Population Datasheet 2022*, <https://www.prb.org/wp-content/uploads/2022/09/2022-World-Population-Data-Sheet-Booklet.pdf> (2022).

20 O'Malley, J., Wardlaw, T., You, D., Hug, L. & Anthony, D. Africa's child demographics and the world's future. *Lancet* **384**, 730-732, doi:10.1016/S0140-6736(14)61331-3 (2014).

21 Schutte, C. M. Analysis of HIV-related mortality data in a tertiary South African neurology unit, 2006-2012. *Southern African Journal of HIV Medicine* **14**, 121-124 (2013).

22 Rohlwink, U. K. *et al.* Clinical characteristics and neurodevelopmental outcomes of children with tuberculous meningitis and hydrocephalus. *Dev Med Child Neurol* **58**, 461-468, doi:10.1111/dmcn.13054 (2016).

23 Rohlwink, U. K. *et al.* Tuberculous meningitis in children is characterized by compartmentalized immune responses and neural excitotoxicity. *Nature Communications* **10**, 3767, doi:10.1038/s41467-019-11783-9 (2019).

24 Thrupp, N. *et al.* Single-nucleus RNA-Seq is not suitable for detection of microglial activation genes in humans. *Cell reports* **32**, 108189 (2020).

25 Stuart, T. *et al.* Comprehensive Integration of Single-Cell Data. *Cell* **177**, 1888-1902.e1821, doi:https://doi.org/10.1016/j.cell.2019.05.031 (2019).

26 Kleshchevnikov, V. *et al.* Cell2location maps fine-grained cell types in spatial transcriptomics. *Nat. Biotechnol.* **40**, 661-671, doi:10.1038/s41587-021-01139-4 (2022).

27 Maynard, K. R. *et al.* Transcriptome-scale spatial gene expression in the human dorsolateral prefrontal cortex. *Nat. Neurosci.* **24**, 425-436 (2021).

28 Hintsch, G. *et al.* The calsyntenins—a family of postsynaptic membrane proteins with distinct neuronal expression patterns. *Mol. Cell. Neurosci.* **21**, 393-409 (2002).

29 Aevermann, B. *et al.* A machine learning method for the discovery of minimum marker gene combinations for cell type identification from single-cell RNA sequencing. *Genome Res.* **31**, 1767-1780 (2021).

30 Aevermann, B. D. *et al.* Cell type discovery using single-cell transcriptomics: implications for ontological representation. *Hum. Mol. Genet.* **27**, R40-R47, doi:10.1093/hmg/ddy100 (2018).

31 Tan, S. Z. K. *et al.* Brain Data Standards - A method for building data-driven cell-type ontologies. *Sci Data* **10**, 50, doi:10.1038/s41597-022-01886-2 (2023).

32 Chen, K. H., Boettiger, A. N., Moffitt, J. R., Wang, S. & Zhuang, X. Spatially resolved, highly multiplexed RNA profiling in single cells. *Science* **348**, aaa6090, doi:doi:10.1126/science.aaa6090 (2015).

859 33 Love, M. I., Huber, W. & Anders, S. Moderated estimation of fold change and
860 dispersion for RNA-seq data with DESeq2. *Genome biology* **15**, 1-21 (2014).
861 34 Zhao, E. *et al.* Spatial transcriptomics at subspot resolution with BayesSpace. *Nat.*
862 *Biotechnol.* **39**, 1375-1384 (2021).
863 35 Radner, S. *et al.* beta2 and gamma3 laminins are critical cortical basement membrane
864 components: ablation of Lamb2 and Lamc3 genes disrupts cortical lamination and
865 produces dysplasia. *Dev Neurobiol* **73**, 209-229, doi:10.1002/dneu.22057 (2013).
866 36 De Angelis, C. *et al.* Compound heterozygous variants in LAMC3 in association with
867 posterior periventricular nodular heterotopia. *BMC Med Genomics* **14**, 64,
868 doi:10.1186/s12920-021-00911-4 (2021).
869 37 Barak, T. *et al.* Recessive LAMC3 mutations cause malformations of occipital cortical
870 development. *Nat. Genet.* **43**, 590-594, doi:10.1038/ng.836 (2011).
871 38 Wang, Y., Lin, L., Lai, H., Parada, L. F. & Lei, L. Transcription factor Sox11 is essential
872 for both embryonic and adult neurogenesis. *Dev. Dyn.* **242**, 638-653,
873 doi:https://doi.org/10.1002/dvdy.23962 (2013).
874 39 Hoshiba, Y. *et al.* Sox11 Balances Dendritic Morphogenesis with Neuronal Migration
875 in the Developing Cerebral Cortex. *J. Neurosci.* **36**, 5775-5784,
876 doi:10.1523/JNEUROSCI.3250-15.2016 (2016).
877 40 Ling, K. H. *et al.* Molecular networks involved in mouse cerebral corticogenesis and
878 spatio-temporal regulation of Sox4 and Sox11 novel antisense transcripts revealed by
879 transcriptome profiling. *Genome Biol* **10**, R104, doi:10.1186/gb-2009-10-10-r104
880 (2009).
881 41 Kakimoto, T., Katoh, H. & Negishi, M. Regulation of neuronal morphology by Toca-1,
882 an F-BAR/EFC protein that induces plasma membrane invagination. *J. Biol. Chem.* **281**,
883 29042-29053 (2006).
884 42 Winsky-Sommerer, R., King, H. A., Iadevaia, V., Moller-Levet, C. & Gerber, A. P. A post-
885 transcriptional regulatory landscape of aging in the female mouse hippocampus. *Front*
886 *Aging Neurosci* **15**, 1119873, doi:10.3389/fnagi.2023.1119873 (2023).
887 43 Twohig, J. P. *et al.* Age-dependent maintenance of motor control and corticostriatal
888 innervation by death receptor 3. *J. Neurosci.* **30**, 3782-3792,
889 doi:10.1523/JNEUROSCI.1928-09.2010 (2010).
890 44 Yang, Q. Q. *et al.* Nuclear isoform of FGF13 regulates post-natal neurogenesis in the
891 hippocampus through an epigenomic mechanism. *Cell Rep* **35**, 109127,
892 doi:10.1016/j.celrep.2021.109127 (2021).
893 45 Wu, Q.-F. *et al.* Fibroblast growth factor 13 is a microtubule-stabilizing protein
894 regulating neuronal polarization and migration. *Cell* **149**, 1549-1564 (2012).
895 46 Zhang, X., Lin, P.-Y., Liakath-Ali, K. & Südhof, T. C. Teneurins assemble into presynaptic
896 nanoclusters that promote synapse formation via postsynaptic non-teneurin ligands.
897 *Nature Communications* **13**, 2297 (2022).
898 47 Cheung, A. *et al.* Teneurin paralogues are able to localise synaptic sites driven by the
899 intracellular domain and have the potential to form cis-heterodimers. *Front Neurosci*
900 **16**, 915149, doi:10.3389/fnins.2022.915149 (2022).
901 48 Beckmann, J., Schubert, R., Chiquet-Ehrismann, R. & Müller, D. J. Deciphering teneurin
902 domains that facilitate cellular recognition, cell–cell adhesion, and neurite outgrowth
903 using atomic force microscopy-based single-cell force spectroscopy. *Nano Lett.* **13**,
904 2937-2946 (2013).

49 Khatir, I. *et al.* Decoupling of mRNA and Protein Expression in Aging Brains Reveals the Age-Dependent Adaptation of Specific Gene Subsets. *Cells* **12**, doi:10.3390/cells12040615 (2023).
50 Patel, K. G., Liu, C., Cameron, P. L. & Cameron, R. S. Myr 8, a novel unconventional myosin expressed during brain development associates with the protein phosphatase catalytic subunits 1alpha and 1gamma1. *J. Neurosci.* **21**, 7954-7968, doi:10.1523/JNEUROSCI.21-20-07954.2001 (2001).
51 Jansen, L. A. *et al.* PI3K/AKT pathway mutations cause a spectrum of brain malformations from megalencephaly to focal cortical dysplasia. *Brain* **138**, 1613-1628, doi:10.1093/brain/awv045 (2015).
52 Cruz, E., Bessieres, B., Magistretti, P. & Alberini, C. M. Differential role of neuronal glucose and PFKFB3 in memory formation during development. *Glia* **70**, 2207-2231, doi:10.1002/glia.24248 (2022).
53 Irvin, D. K., Zurcher, S. D., Nguyen, T., Weinmaster, G. & Kornblum, H. I. Expression patterns of Notch1, Notch2, and Notch3 suggest multiple functional roles for the Notch-DSL signaling system during brain development. *J. Comp. Neurol.* **436**, 167-181 (2001).
54 Tanaka, M., Kadokawa, Y., Hamada, Y. & Marunouchi, T. Notch2 expression negatively correlates with glial differentiation in the postnatal mouse brain. *J. Neurobiol.* **41**, 524-539 (1999).
55 Macnair, W., Gupta, R. & Claassen, M. psupertime: supervised pseudotime analysis for time-series single-cell RNA-seq data. *Bioinformatics* **38**, i290-i298, doi:10.1093/bioinformatics/btac227 (2022).
56 Driessens, S. L. *et al.* Genes associated with cognitive ability and HAR show overlapping expression patterns in human cortical neuron types. *Nature communications* **14**, 4188 (2023).
57 Gauvain, M. *Cognitive development in infancy and childhood*. (Cambridge University Press, 2022).
58 Lee, J. J. *et al.* Gene discovery and polygenic prediction from a genome-wide association study of educational attainment in 1.1 million individuals. *Nat. Genet.* **50**, 1112-1121, doi:10.1038/s41588-018-0147-3 (2018).
59 Savage, J. E. *et al.* Genome-wide association meta-analysis in 269,867 individuals identifies new genetic and functional links to intelligence. *Nat. Genet.* **50**, 912-919, doi:10.1038/s41588-018-0152-6 (2018).
60 Doan, R. N. *et al.* Mutations in Human Accelerated Regions Disrupt Cognition and Social Behavior. *Cell* **167**, 341-354 e312, doi:10.1016/j.cell.2016.08.071 (2016).
61 Bentourkia, M. h. *et al.* Evolution of brain glucose metabolism with age in epileptic infants, children and adolescents. *Brain and Development* **20**, 524-529, doi:https://doi.org/10.1016/S0387-7604(98)00040-0 (1998).
62 Huttenlocher, P. R. Synaptic density in human frontal cortex - developmental changes and effects of aging. *Brain Res.* **163**, 195-205, doi:10.1016/0006-8993(79)90349-4 (1979).
63 Barnacle, J. R., Davis, A. G. & Wilkinson, R. J. Recent advances in understanding the human host immune response in tuberculous meningitis. *Frontiers in Immunology* **14**, doi:10.3389/fimmu.2023.1326651 (2024).
64 Yang, Q. *et al.* IP-10 and MIG Are Compartmentalized at the Site of Disease during Pleural and Meningeal Tuberculosis and Are Decreased after Antituberculosis

Treatment. *Clinical and Vaccine Immunology* **21**, 1635-1644, doi:doi:10.1128/CVI.00499-14 (2014).

65 Johansen, N. *et al.* Interindividual variation in human cortical cell type abundance and expression. *Science* **382**, eadf2359, doi:10.1126/science.adf2359 (2023).

66 Ximerakis, M. *et al.* Single-cell transcriptomic profiling of the aging mouse brain. *Nat. Neurosci.* **22**, 1696-1708, doi:10.1038/s41593-019-0491-3 (2019).

67 Berg, J. *et al.* Human neocortical expansion involves glutamatergic neuron diversification. *Nature* **598**, 151-158, doi:10.1038/s41586-021-03813-8 (2021).

68 Mohan, H. *et al.* Dendritic and Axonal Architecture of Individual Pyramidal Neurons across Layers of Adult Human Neocortex. *Cereb. Cortex* **25**, 4839-4853, doi:10.1093/cercor/bhv188 (2015).

69 Gidon, A. *et al.* Dendritic action potentials and computation in human layer 2/3 cortical neurons. *Science* **367**, 83-87, doi:10.1126/science.aax6239 (2020).

70 Eyal, G. *et al.* Human Cortical Pyramidal Neurons: From Spines to Spikes via Models. *Front Cell Neurosci* **12**, 181, doi:10.3389/fncel.2018.00181 (2018).

71 Testa-Silva, G. *et al.* High bandwidth synaptic communication and frequency tracking in human neocortex. *PLoS Biol.* **12**, e1002007, doi:10.1371/journal.pbio.1002007 (2014).

72 Beaulieu-Laroche, L. *et al.* Enhanced Dendritic Compartmentalization in Human Cortical Neurons. *Cell* **175**, 643-651 e614, doi:10.1016/j.cell.2018.08.045 (2018).

73 Benyamin, B. *et al.* Childhood intelligence is heritable, highly polygenic and associated with FNBP1L. *Mol. Psychiatry* **19**, 253-258 (2014).

74 Chiang, S.-Y. *et al.* Usp11 controls cortical neurogenesis and neuronal migration through Sox11 stabilization. *Science advances* **7**, eabc6093 (2021).

75 Habib, N. *et al.* Massively parallel single-nucleus RNA-seq with DroNc-seq. *Nat. Methods* **14**, 955-958, doi:10.1038/nmeth.4407 (2017).

76 McGinnis, C. S., Murrow, L. M. & Gartner, Z. J. DoubletFinder: Doublet Detection in Single-Cell RNA Sequencing Data Using Artificial Nearest Neighbors. *Cell Syst* **8**, 329-337 e324, doi:10.1016/j.cels.2019.03.003 (2019).

77 DePasquale, E. A. K. *et al.* DoubletDecon: Deconvoluting Doublets from Single-Cell RNA-Sequencing Data. *Cell Rep* **29**, 1718-1727 e1718, doi:10.1016/j.celrep.2019.09.082 (2019).

78 Raudvere, U. *et al.* g:Profiler: a web server for functional enrichment analysis and conversions of gene lists (2019 update). *Nucleic Acids Res.* **47**, W191-W198, doi:10.1093/nar/gkz369 (2019).

79 Bunis, D. G., Andrews, J., Fragiadakis, G. K., Burt, T. D. & Sirota, M. dittoSeq: universal user-friendly single-cell and bulk RNA sequencing visualization toolkit. *Bioinformatics* **36**, 5535-5536, doi:10.1093/bioinformatics/btaa1011 (2020).

80 Wickham, H. *ggplot2: elegant graphics for data analysis*. (Springer, 2016).

81 Ouyang, J. F., Kamaraj, U. S., Cao, E. Y. & Rackham, O. J. L. ShinyCell: simple and sharable visualization of single-cell gene expression data. *Bioinformatics* **37**, 3374-3376, doi:10.1093/bioinformatics/btab209 (2021).

82 Tippani, M. *et al.* Vistoseg: a matlab pipeline to process, analyze and visualize high resolution histology images for visium spatial transcriptomics data. *bioRxiv* (2021).

83 Choi, H. M. *et al.* Mapping a multiplexed zoo of mRNA expression. *Development* **143**, 3632-3637, doi:10.1242/dev.140137 (2016).

Data Availability

All scripts used to analyse the data are indicated in the methods section and are available in the supplementary material. A description of the raw and analysed data files will be made available on the University of Cape Town's ZivaHub data sharing platform on publication. As the data is from living donors, access to the data will be mediated through contact with the corresponding author. A ShinyApp will be made publicly available on publication for exploration of the annotated snRNA-seq data.

Acknowledgments

This research was support by a Royal Society/Global Challenges Research Fund/African Academy of Sciences Future Leaders African Independent Researcher (FLAIR) Fellowship to D.H. (FLR\R1\191008), a Royal Society/Global Challenges Research Fund FLAIR Collaboration grant to T.S.S. and D.H. (FCG\R1\201023), a National Research Foundation (NRF) Research Development Grant for Y-rated Researchers Award to DH (CSRP210415595025), a University of Cape Town (UCT) Building Research Active Academic Staff Grant award to D.H. and a National Institutes of Health (NIH) R21 Exploratory/Development Grant to D.H., J.V.R., C.G.D. and M.J. (TW011225). C.S. was supported by a Harry Crossley Research Scholarship, an Oppenheimer Memorial Trust scholarship, an NRF scholarship and a UCT Vice Chancellor's Research Scholarship. S.F. was supported by a DAAD-NRF joint In-country Scholarship and a UCT Vice Chancellor's Research Scholarship. M.B.V. was supported by an EMBO long-term fellowship (ALTF 415-2018) and a Claude Leon Foundation research fellowship. A.F. was supported by the NRF SARChI Chair of Clinical Neurosciences. Computations were performed using facilities provided by the University of Cape Town's ICTS High Performance Computing team: hpc.uct.ac.za. This publication is part of the Human Cell Atlas: www.humancellatlas.org/publications/

Contributions

C.S. and S.F. conducted the snRNA-seq experiments. C.S. conducted the majority of snRNA-seq analyses. R.M. conducted the Visium and HCR experiments and analysis. J.M. conducted additional HCR experiments. S.Q. provided additional bioinformatics support. M.B.V. liaised with neurosurgeons and prepared all neurosurgical brain tissue samples. R.M., J.B. and J.M.N.E conducted the neurosurgeries and provided donor metadata. C.S., T.S.S., M.G. and D.H. conceptualised, conducted and analysed the MERFISH experiments. U.K.R., M.Z., J.V.R, C.G.D, A.F, and D.H. conceptualised the study and raised funds. D.H., C.S. and R.M wrote the manuscript. D.H. conducted additional analyses and supervised the project. All authors read and commented on the manuscript.

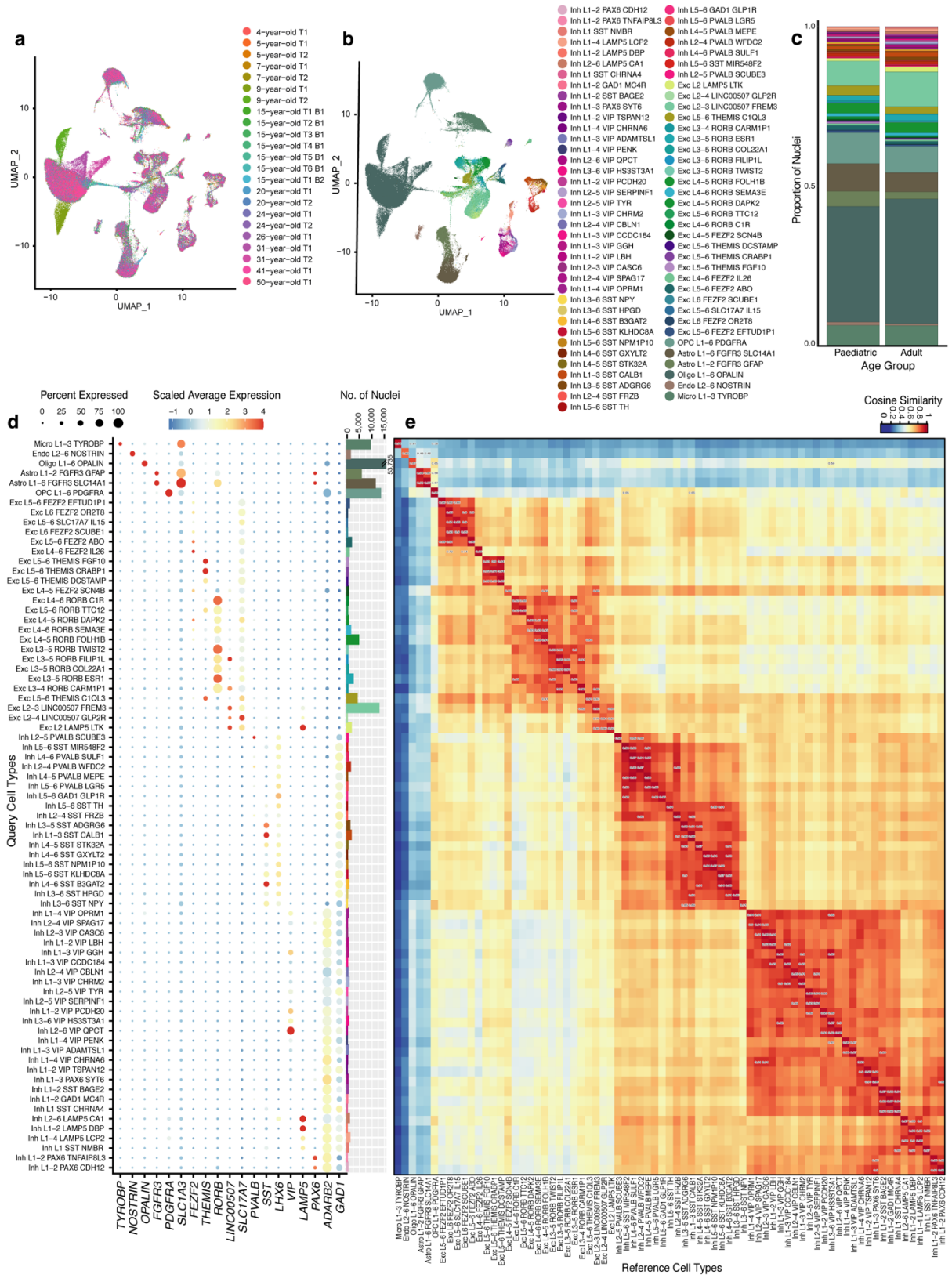

Fig. 1: Annotation of nuclei by label transfer identifies 75 cell types across the 23 datasets. a, Data integration shows alignment of nuclei across the technical (T) and biological (B) replicates from donors ranging in age from 4 to 50 years. **b**, UMAP plot annotated to show the 75 cell types from the Allen Brain Map MTG atlas after filtering to retain nuclei with high confidence annotations. Each cell type is annotated with 1) a major cell class (e.g. Exc for excitatory neuron), 2) the cortical layer the cell is associated with (e.g. L2 for layer 2), 3) a subclass marker gene and 4) a cluster-specific marker gene. **c**, Stacked barplot showing the proportion of nuclei per cell type for each age category out of the total number of nuclei for each group. The cell types are coloured as in **b.** See Extended Data Table 3 for details of statistical tests performed. **d**, Validation of the high-resolution cell type annotations shows a high degree of correspondence in the expression of known cell type-specific marker genes (x axis) with their expected cell type (y axis) (left). The number of nuclei per cell type is shown on the right. **e**, Correlation plot showing the cosine similarity scores assessing similarity between the annotated cell types in our dataset (y axis as in **d**) and the MTG reference dataset (x axis) based on the log normalized expression counts of the top 2000 shared highly variable features between query and reference datasets.

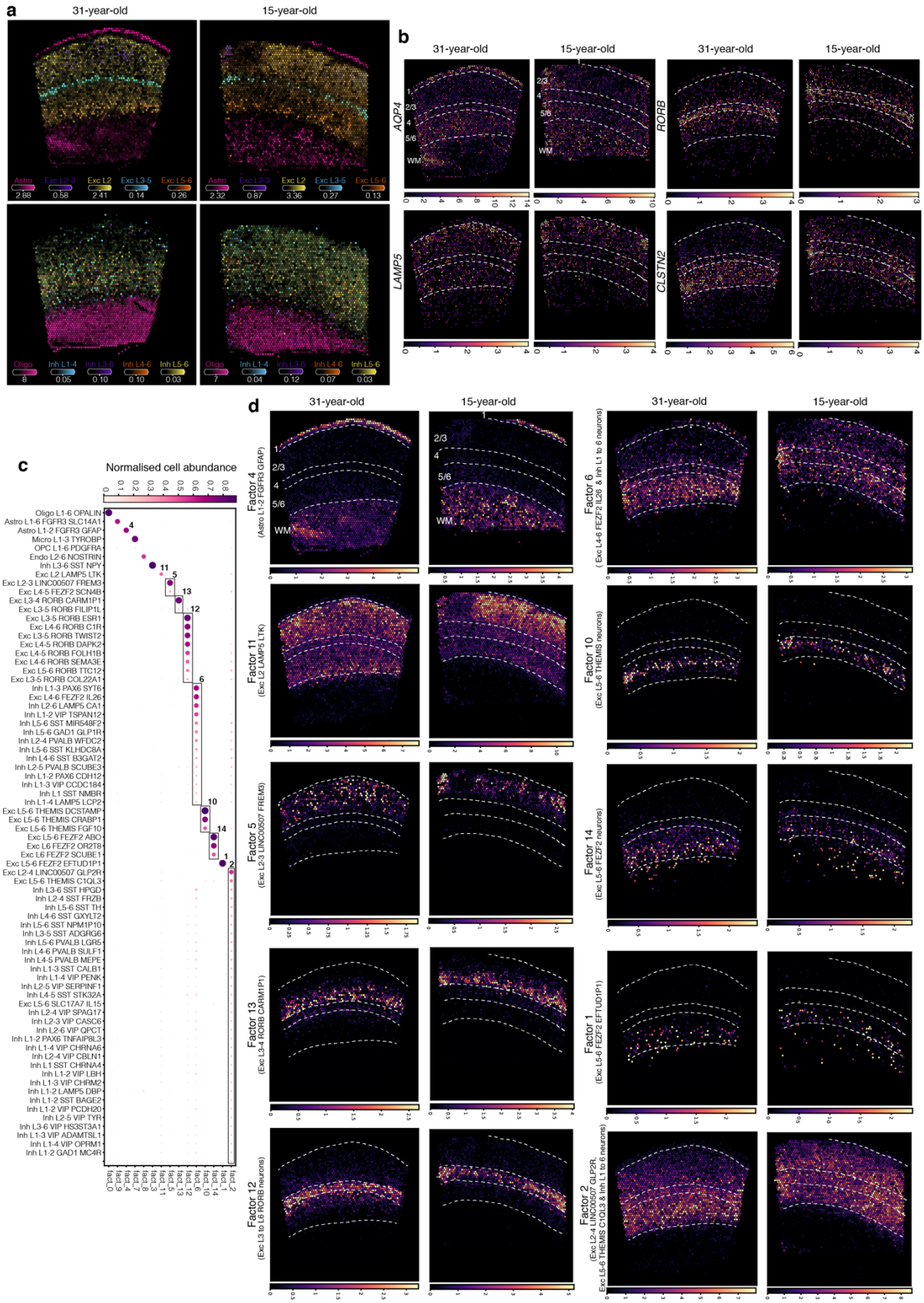

Fig. 2: Visium spatial transcriptomics in the adult and paediatric temporal cortex validates snRNA-seq annotation. **a**, Estimated cell type abundances (colour intensity) in the 31-year-old and 15-year-old temporal cortex tissue sections for a selection of cell types including non-neuronal cell types, excitatory neurons (top row) and inhibitory neurons (bottom row). **b**, Visium gene expression profiles (colour intensity) for a selection of known cortical layer marker genes in the 31-year-old and 15-year-old temporal cortex tissue sections including *AQP4* (layer 1), *LAMP5* (layer 2), RORB (layer 4) and *CLSTN2* (layer 5-6). **c**,**d**, Identification of co-locating cell types using NMF. The dot plot (**c**) shows the NMF weights of the cell types (rows) across each of the NMF factors (columns), which correspond to tissue compartments. Block boxes indicate cell types that co-locate within the indicated compartments. Spatial plots show (**d**) show the NMF weights for selected NMF factor/tissue compartment across the 31-year-old and 15-year-old temporal cortex tissue sections. Panels are displayed in the same order as the dotplot in (**c**), with the dominant cell types for each factor indicated in brackets. Dashed white lines and numbers indicate estimated cortical layer boundaries as indicated in the first two panels of **b** and **d**. WM: white matter. See also Extended Data Figs 4-6.

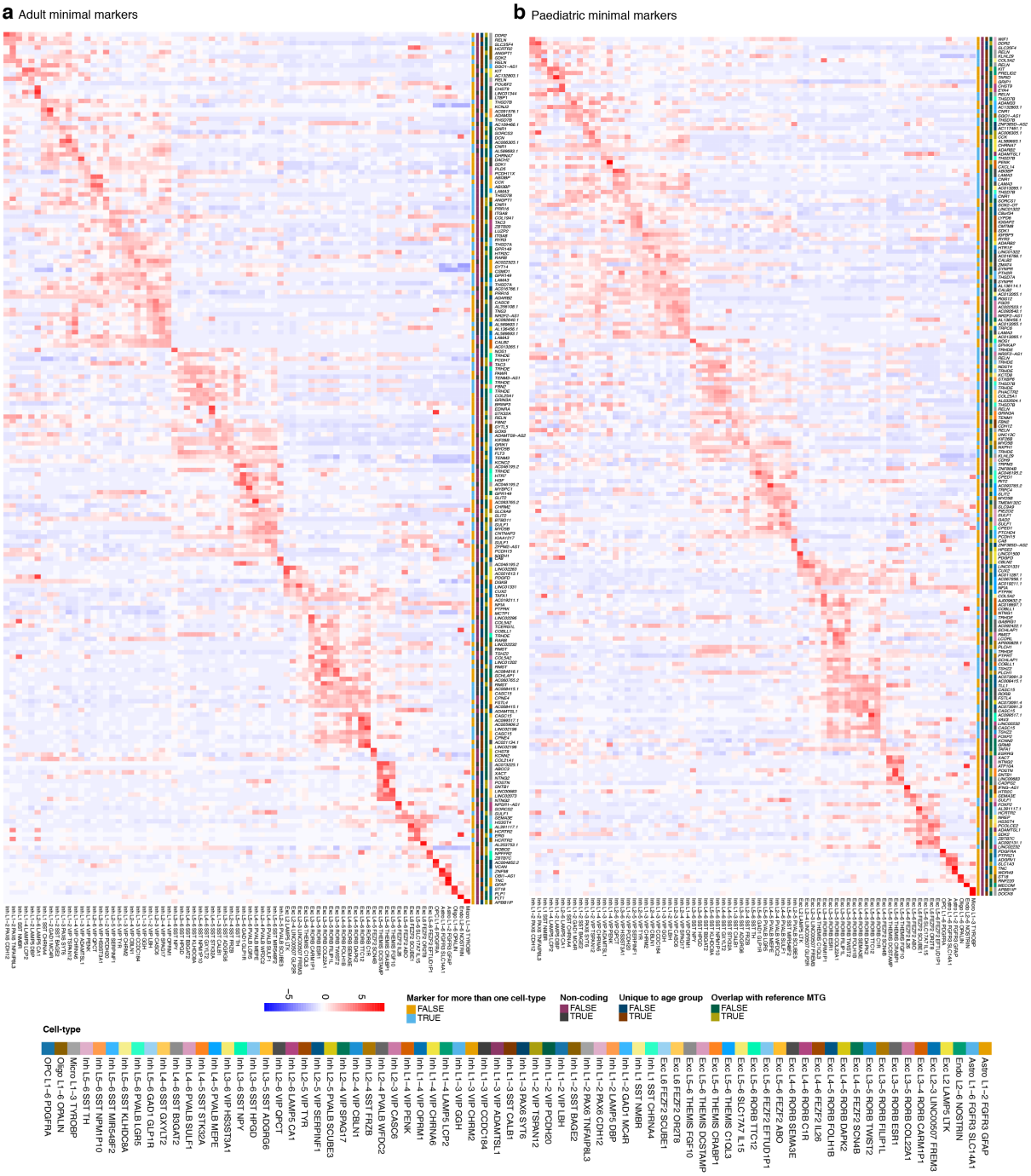

Fig. 3: NS-Forest identifies minimal marker genes distinguishing the cell types in the paediatric and adult temporal cortex snRNA-seq datasets. a,**b**, Heatmap showing the scaled average normalised expression counts of the NS-Forest minimal marker genes (y-axis) identified for 75 cortical cell types (x-axis) across the six adult (**a**) and six paediatric (**b**) datasets. As input into NS-Forest, the nuclei of each sample were randomly down-sampled to the size of the sample with the fewest nuclei. Heatmaps show gene expression values for the down-sampled datasets. The minimal marker genes are annotated (colour codes on the y-axes) according to whether they are unique to a given cell type, whether they are coding/non-coding genes, whether they are unique to the indicated age group, whether they overlap with existing MTG minimal marker gene sets for the same cell type, and according to the cell type they define.

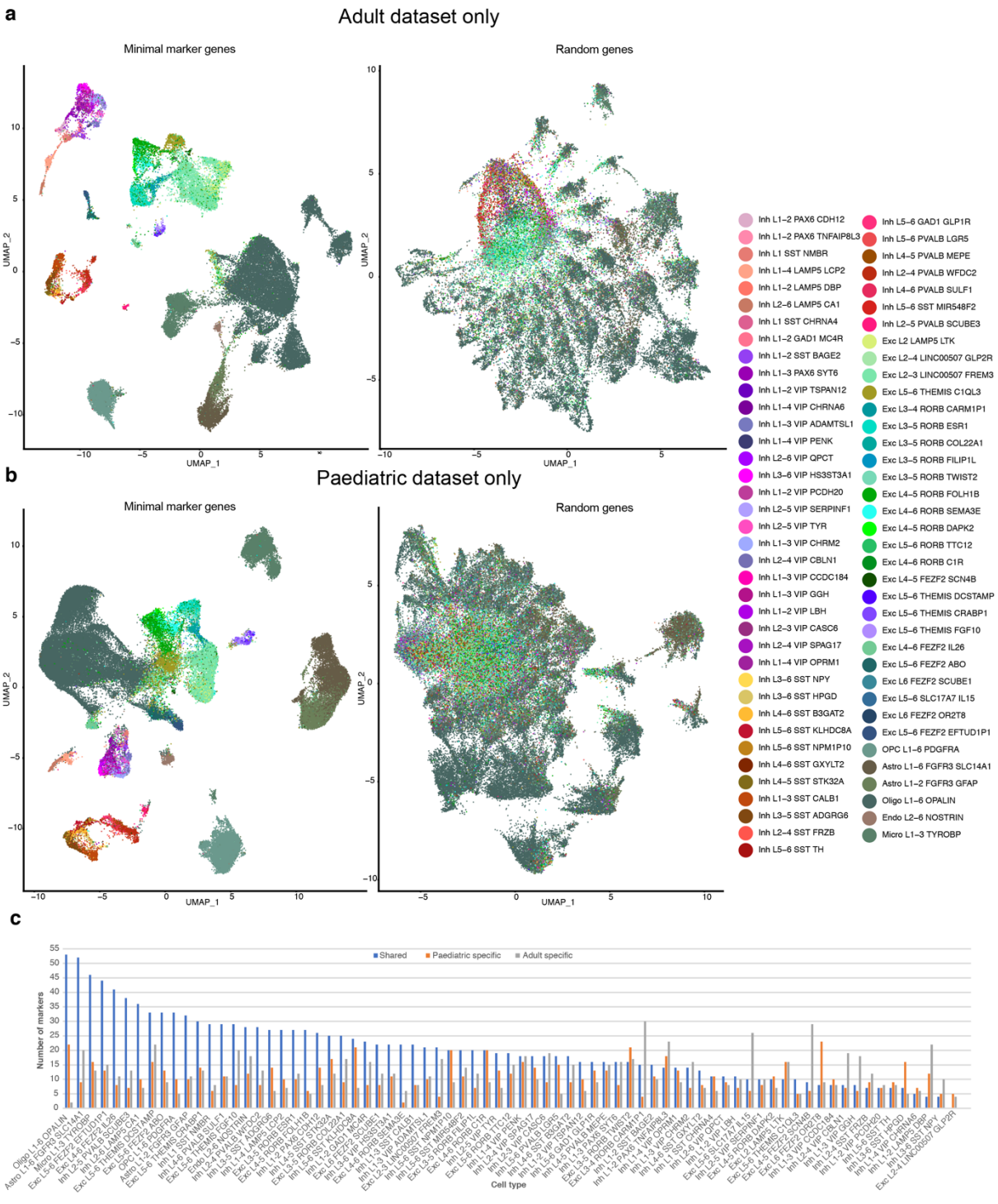

Fig. 4: Validation of NS-Forest minimal markers and assessment of the top NS-forest markers. a,**b**, Annotated UMAP plots following data integration using either the minimal marker genes (left) or the equivalent number of a random set of genes (right) as anchors for the adult (**a**) and paediatric (**b**) datasets. The colour scheme for the cell types is in accordance with the MTG cell taxonomy. **c**, Overlap of the paediatric and adult NS-Forest markers with a high binary expression score (> 0.7) per cell type. The bar plot shows the number of shared markers between paediatric and adult datasets (blue), the number of markers unique to the paediatric datasets (orange), and the number of markers unique to the adult datasets (grey) for each cell type.

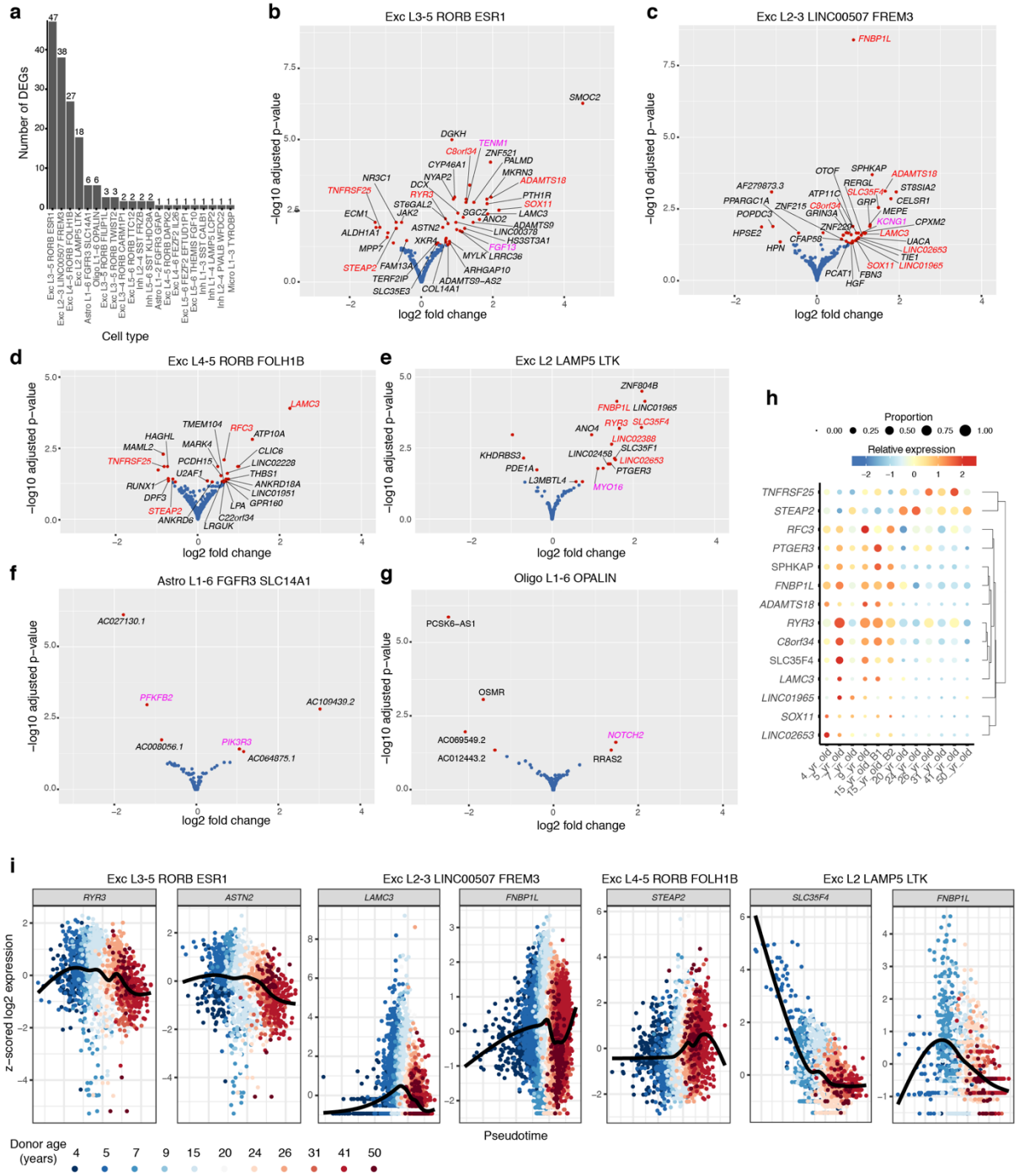

Fig. 5: Differential expression analysis reveals genes guiding temporal cortex maturation. a, 21 cell types with DEGS. **b-g**, Volcano plots showing $\log_2$FoldChange (x axis) and -$\log_{10}$padj values (y axis) for all DESeq2-tested genes in Exc_L3-5_RORB_ESR1, Exc L2-3_LINC00507_FREM3, Exc_L4-5_RORB_FOLH1B, Exc_L2_LAMP5_LTK, Astro_L1-6_FGFR3_SLC14A1 and Oligo L1-6 OPALIN. Red dots indicate genes that were significantly upregulated or downregulated in paediatric samples (padj<0.05 & abs($\log_2$FoldChange)>10%) and selected genes are labelled. Red labels indicate DEGs shared between neuronal cell types. Magenta labels indicate DEGS not shared between cell types that are discussed in the text. Blue dots indicate non-significant genes (padj>0.05 or abs($\log_2$FoldChange)<10%). **h**, Dot plot showing the scaled average normalised expression across samples for DEGS shared between Exc_L3-5_RORB_ESR1, Exc L2-3_LINC00507_FREM3, Exc_L4-5_RORB_FOLH1B, Exc_L2_LAMP5_LTK, Exc_L3-4_RORB_CARM1P1 and Exc_L3-5_RORB_FILIP1L**. i**, psupertime gene expression trajectories for selected DEGs in the indicated cell types. The *x*-axis is the calculated psupertime value for each cell, coloured by sample of origin. The black lines are smoothened curves fit by geom_smooth in the R package ggplot2.

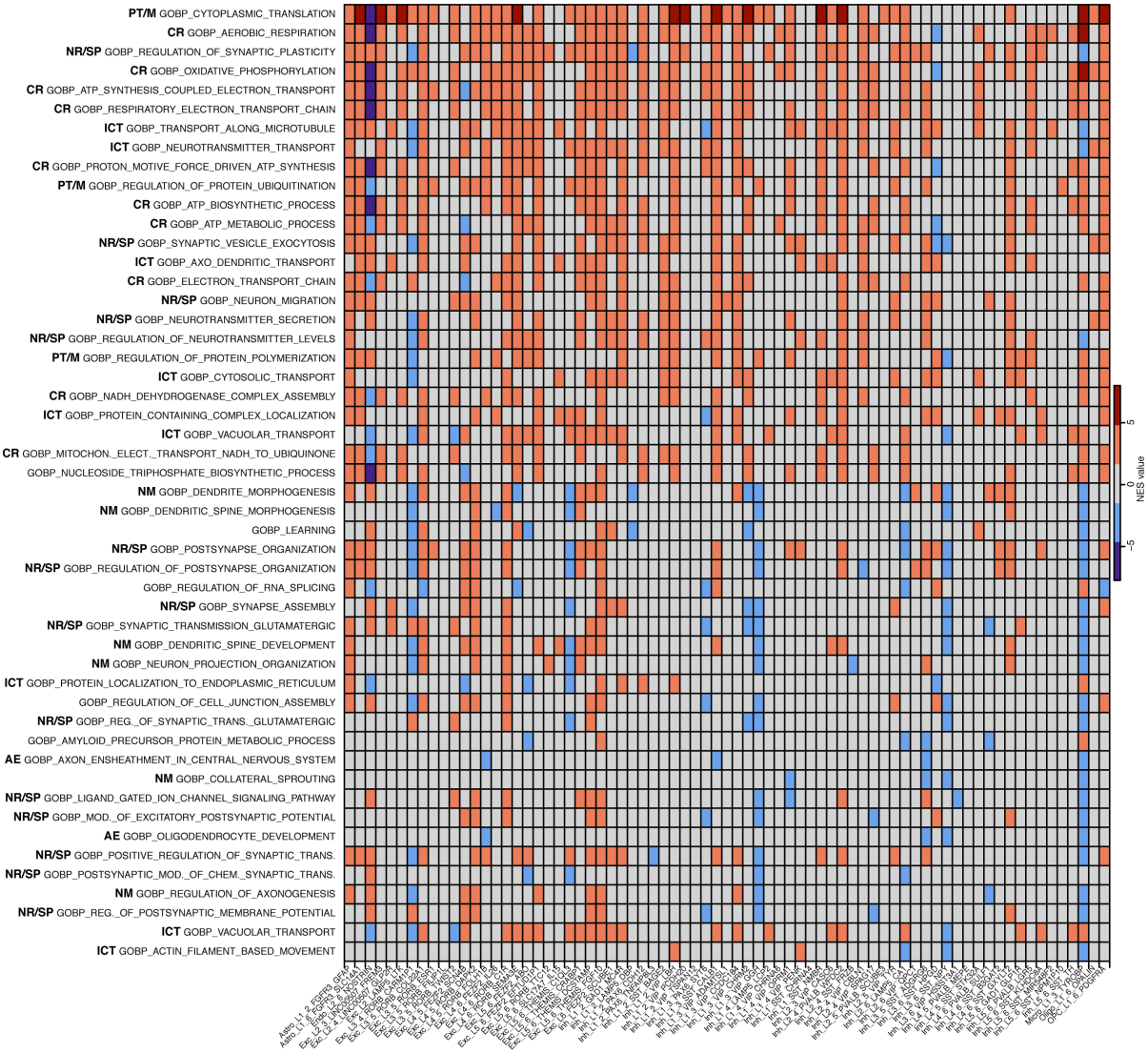

Fig. 6: Pathways that are enriched or depleted across multiple cell types in paediatric samples. GSEA heatmap showing the top 25 most frequently enriched (top 25 rows) or depleted (bottom 25 rows) terms appearing across all cell types. Abbreviations in bold indicate the following categories as referred to in the text: AE, axon ensheathment; CR, cellular respiration; ICT, intracellular transport; NM, neuronal morphogenesis; NR/SP, neurotransmitter release/synaptic plasticity; PT/M, protein translation/modification. Only significantly ($p < 0.01$ and $q < 0.1$) terms are shown. NES value represents the normalized enrichment scores. Grey indicates that the term was not significantly enriched or depleted in the indicted cell type. See also Extended Data Table 12.

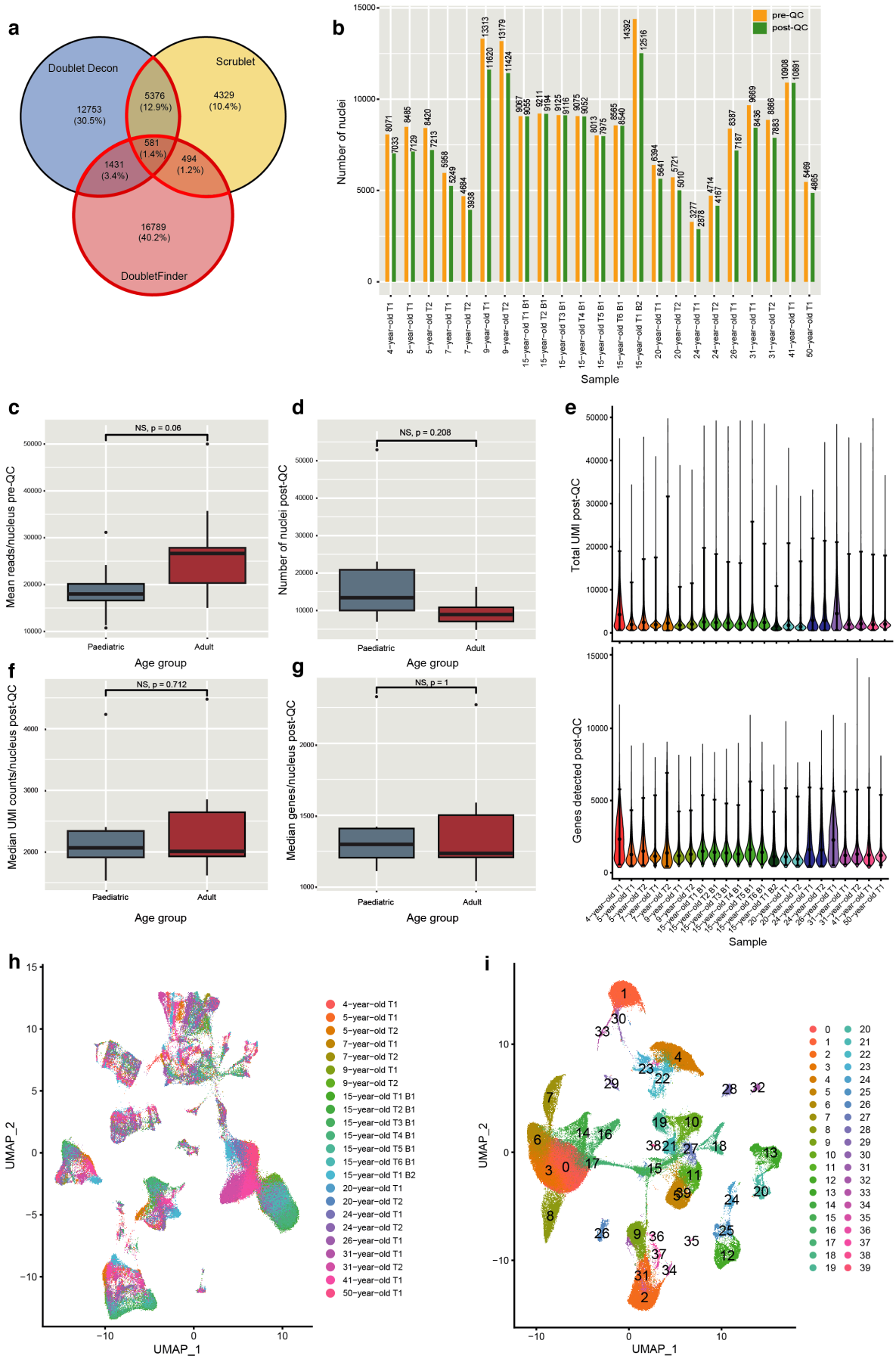

Extended Data Fig. 1: Nuclei quality control (QC) and clustering. a, Number of doublets identified across all 23 datasets by DoubletDecon, DoubletFinder, and Scrublet. Red outline indicates the subset of barcodes called as doublets that were removed. **b**, Total number of nuclei per dataset before (yellow) and after (green) QC. **c**, Mean number of reads per nucleus (y axis) by dataset before QC split by age group (x axis). p value determined by two-tailed Welch's t-test. **d**, Number of nuclei (y axis) by sample after QC split by age group (x axis). p value determined by Brunnermunzel permutation test**. e**, Violin plots showing the number of unique molecular identifiers (UMIs) (top) and the number of genes detected (bottom) per nucleus per sample after QC. Black dots indicate the median value. Error bars show 95% confidence intervals. **f**,**g**, Median number of UMIs (2,263 paediatric and 2,011 adult) (**f**) and the median number of genes (1,372 paediatric and 1,226 adult) (**g**) detected

per nucleus (y axes) by sample after QC split by age group (x axis). p values determined by two-tailed Brunnermunzel permutation test. **h**, UMAP plot for the 23 datasets prior to integration. **i**, UMAP plot showing the resulting clusters determined by the shared nearest neighbour algorithm. Data in all box plots represent mean ± sem for six paediatric and six adult samples. No significant differences were detected between paediatric and adult samples. B, biological replicate; NS, not significant; T, technical replicate. See also Extended Data Table 2.

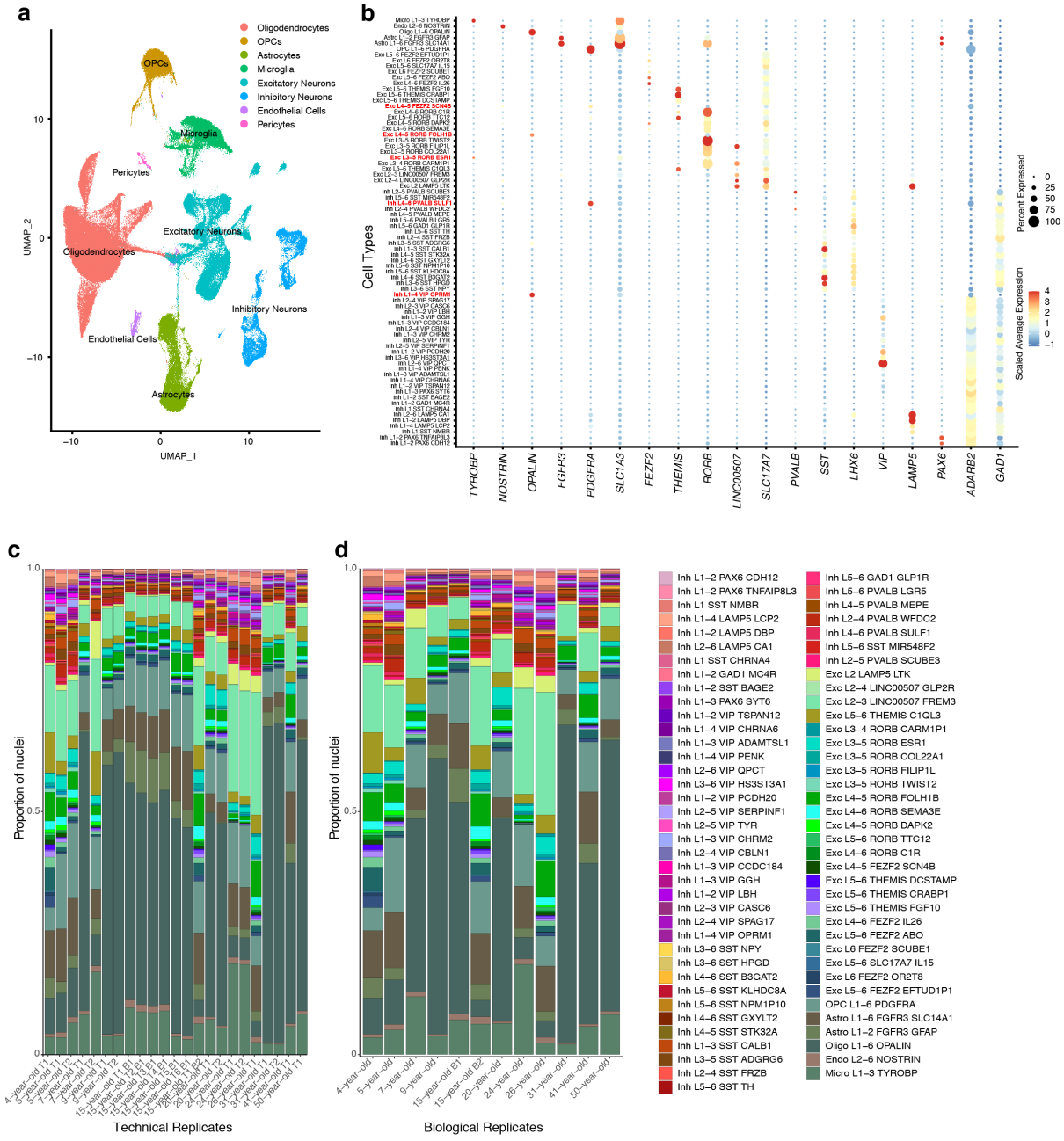

Extended Data Fig. 2: Annotation and assessment of cell composition across datasets. a, UMAP plot showing cluster annotation at the level of major brain cell types (level 1 annotation). **b**, Examination of known cell type-specific marker genes (x axis) after label transfer classify each nucleus according to the Allen Brain Map MTG atlas[1] (level 2 annotation) (y axis) (left). Off-target gene expression is evident in several cell types (marked in red), which is likely due to multiplets or nuclei contaminated with ambient mRNA. **c-d**, Stacked barplots after filtering to retain nuclei with high confidence annotations showing the proportion of nuclei per cell type (y axis) for each technical replicate (**c**) or biological replicate (**d**) (x axis) out of the total number of nuclei for each group. Samples with technical replicates showed high degrees of similarity in cell composition between their replicates (**c**). Technical replicates from each donor were merged to allow comparisons between the 12 samples (**d**).

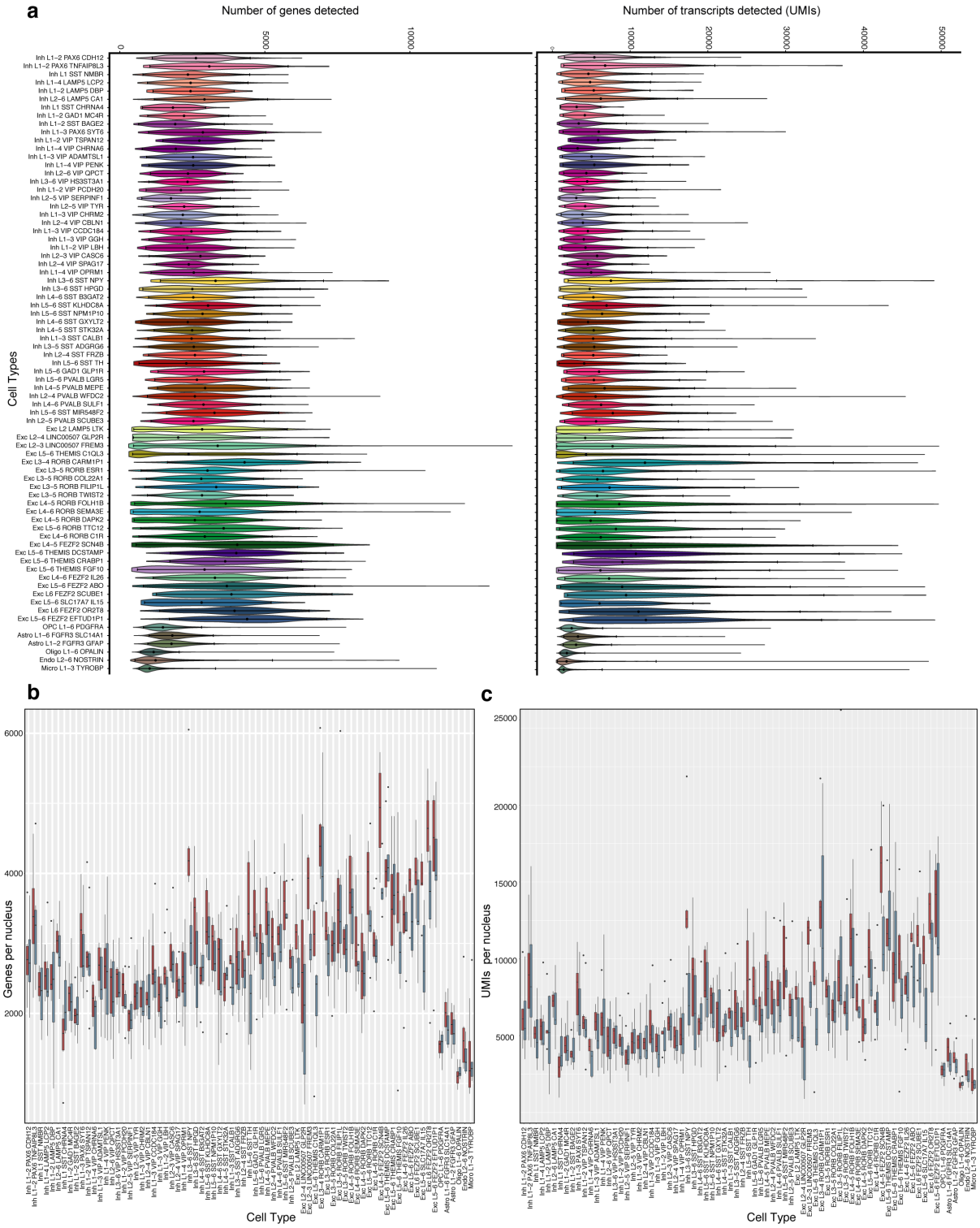

Extended Data Fig. 3: Assessment of the sequencing metrics for the annotated cell types. a, Violin plots showing the distribution of the number of genes (left) and transcripts (right) detected per nucleus per cell type across all datasets. Black dots indicate the median value. Error bars show 95% confidence intervals. **b**,**c**, Boxplots showing the number of genes (**b**) and the number of UMIs (**c**) (y axis) detected per cell type per sample (x axis) split by age group (red: adult, grey: paediatric). Data in all box plots represent mean ± sem for six paediatric and six adult samples for each cell type. No significant differences were detected (i.e. padj > 0.05). See Extended Data Table 3 for details of statistical tests performed.

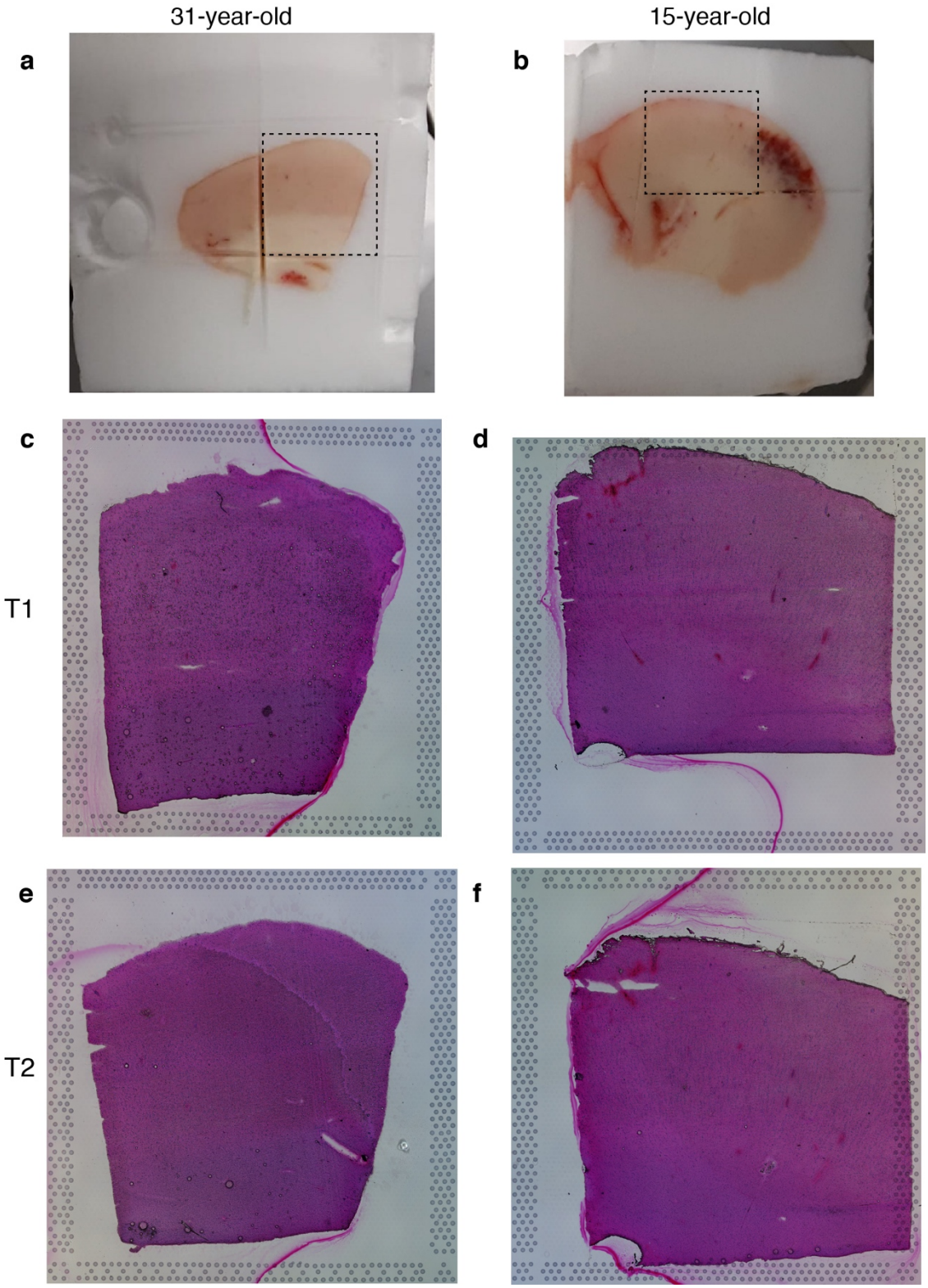

Extended Data Fig. 4: Visium Spatial Gene Expression samples. a,**b**, 31-year-old (**a**) and 15-year-old (**b**) temporal cortex tissue blocks embedded in OCT. Black dashed boxes outline the regions collected onto the Visium Spatial Gene Expression slide. **c**-**f**, H&E stained technical replicate tissue sections used to generate Visium Spatial Gene Expression libraries for the 31-year-old (**c**,**e**) and 15-year-old (**d**,**f**) tissue samples. T, technical replicate.

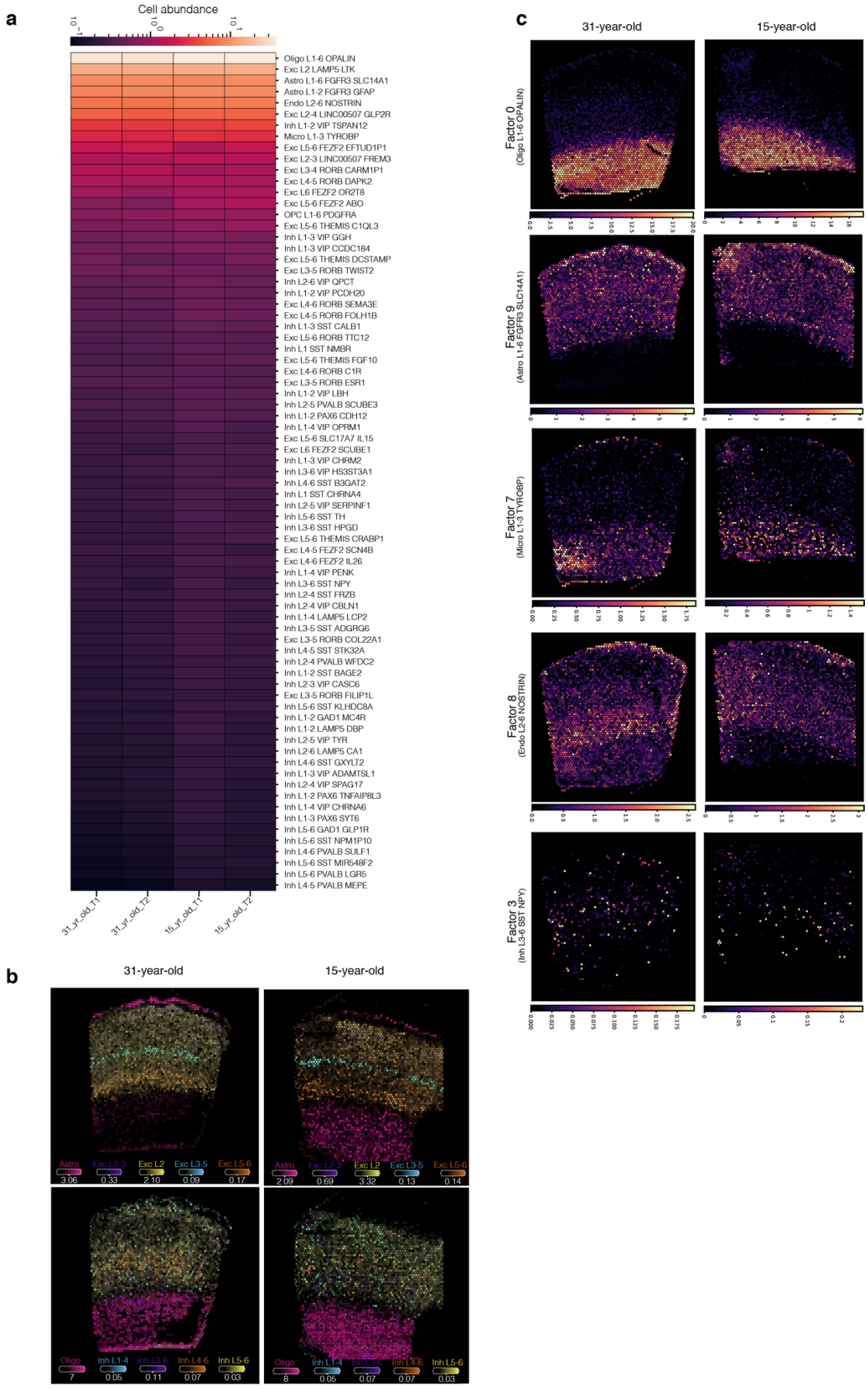

Extended Data Fig. 5: Spatial mapping of cell types in the human temporal cortex. a, Estimated cell abundance of 75 cell types across all Visium samples. Shown is a heatmap with the colour indicating the relative cell abundance of cell types (rows) across the different samples (columns). **b**, Estimated cell type abundances (colour intensity) in the technical replicate 31-year-old and 15-year-old temporal cortex tissue sections for a selection of cell types including non-neuronal cell types, excitatory neurons (top row) and inhibitory neurons (bottom row). **d**, Spatial plots show of the NMF weights for selected NMF factor/tissue compartment across the 31-year-old and 15-year-old temporal cortex tissue sections. Panels are displayed in the same order as the dotplot in Fig. 2c, with the dominant cell types for each factor indicated in brackets. T, technical replicate.

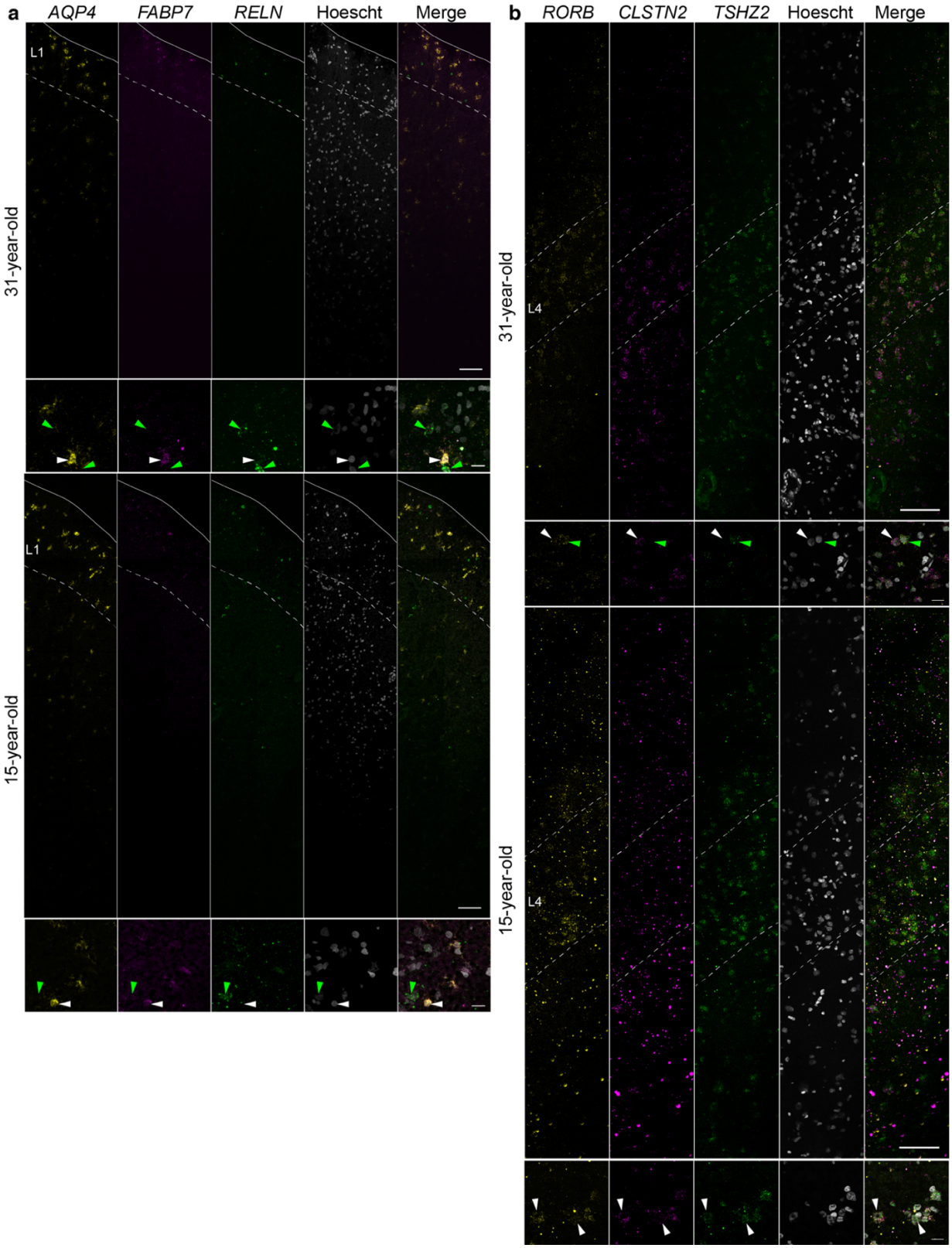

Extended Data Fig. 6: *In situ* HCR analysis of selected cortical layer marker genes. Expression of **a**, layer 1 markers *AQP4*, *FABP7* and *RELN* and **b**, layer 4-6 markers *RORB*, *CLSTN2* and *TSHZ2* in frozen temporal cortex tissue sections from the same 31-year-old and 15-year-old donor tissue used for Visium. High magnification views of layer 1 in **a** indicate *AQP4*/*RELN*-positive cells (yellow arrowheads) and *FABP7* positive cells (green arrowhead). In high magnification views of layer 4 in **b** in the 31-year-old tissue section, *RORB*/*CLSTN2*-positive (white arrowhead) and *RORB*/*TSHZ2*-positive cells (green arrowhead) are indicated. In high magnification views of layer 4 in **b** in the 15-year-old tissue section *RORB*/*CLSTN2*/*TSHZ2*-positive cells (white arrowheads) are indicated. Dashed white lines indicate layer boundaries. Solid white line indicates tissue edge. Scale bars are 100 µm in low magnification views (tile scan at 40x) and 20 µm in high magnification views (63x).

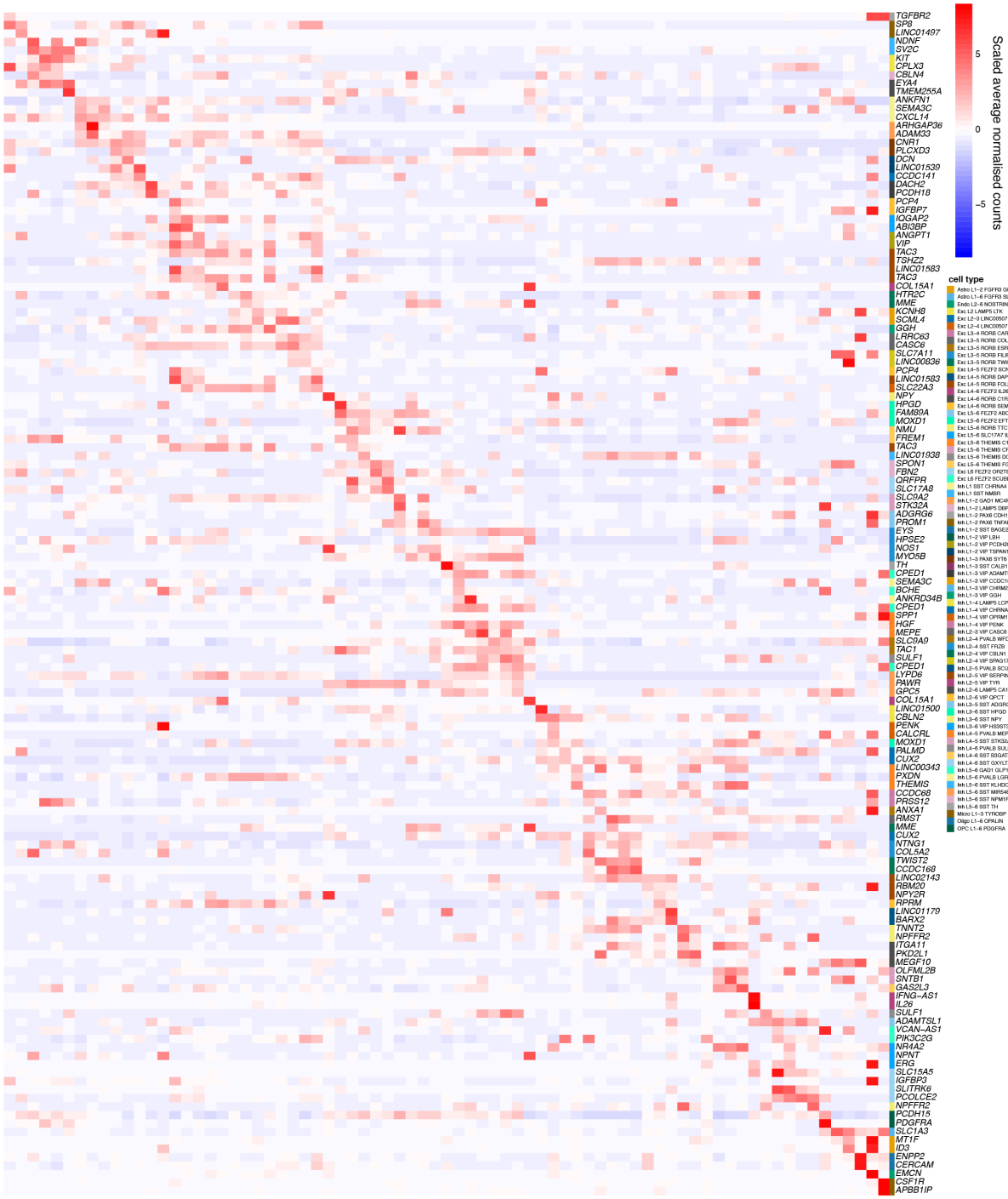

Extended Data Fig. 7: Expression of the reference MTG atlas minimal markers. Heatmap showing the scaled average normalised expression counts of the NS-Forest minimal marker genes identified for the reference MTG cell atlas dataset (y-axis) in each of the 75 query cortical cell types identified in the combined adult and paediatric snRNA-seq datasets (x-axis). The minimal marker genes are annotated (colour codes on the y-axes) according to the cell type they define.

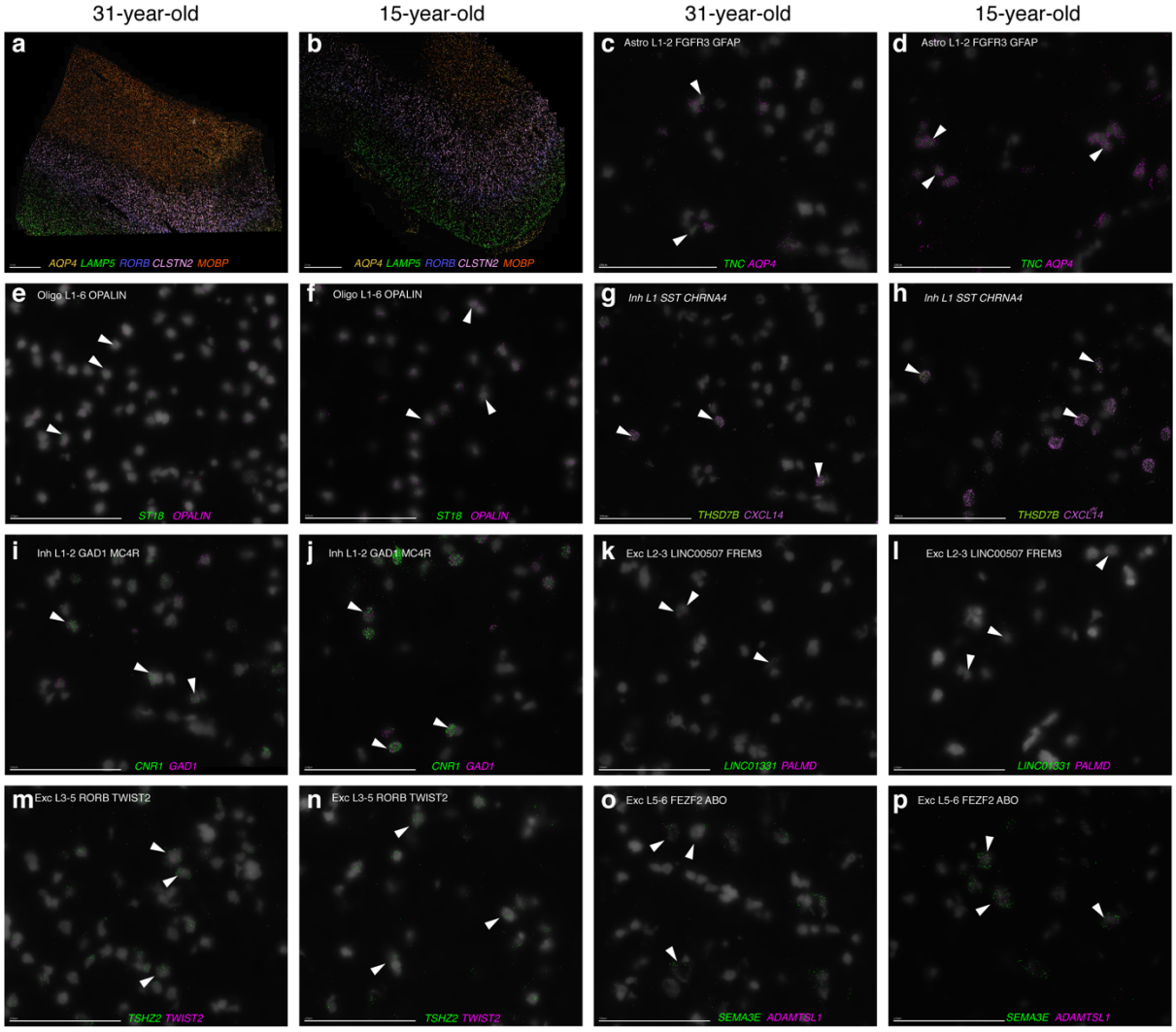

Extended Data Fig. 8: MERFISH spatial transcriptomics analysis of selected NS-forest markers. a, **b** Low magnification views of the 31-year-old (a) and 15-year-old (b) MERFISH datasets showing the expression of known layer maker genes in the expected layers as validation of the MERFISH experiment. **c**-**p**, High magnification views of 31-year-old (c,e,g,l,k,m,o) and 15-year-old (d,f,h,j,l,n,p) MERFISH datasets showing the overlap of new NS-Forest minimal markers (green) with published NS-Forest minimal markers (magenta) in indicated cells (arrowheads). The cell type that the NS-Forest markers are associated with is indicated in the top left corner. Scale bars: 100 µm.

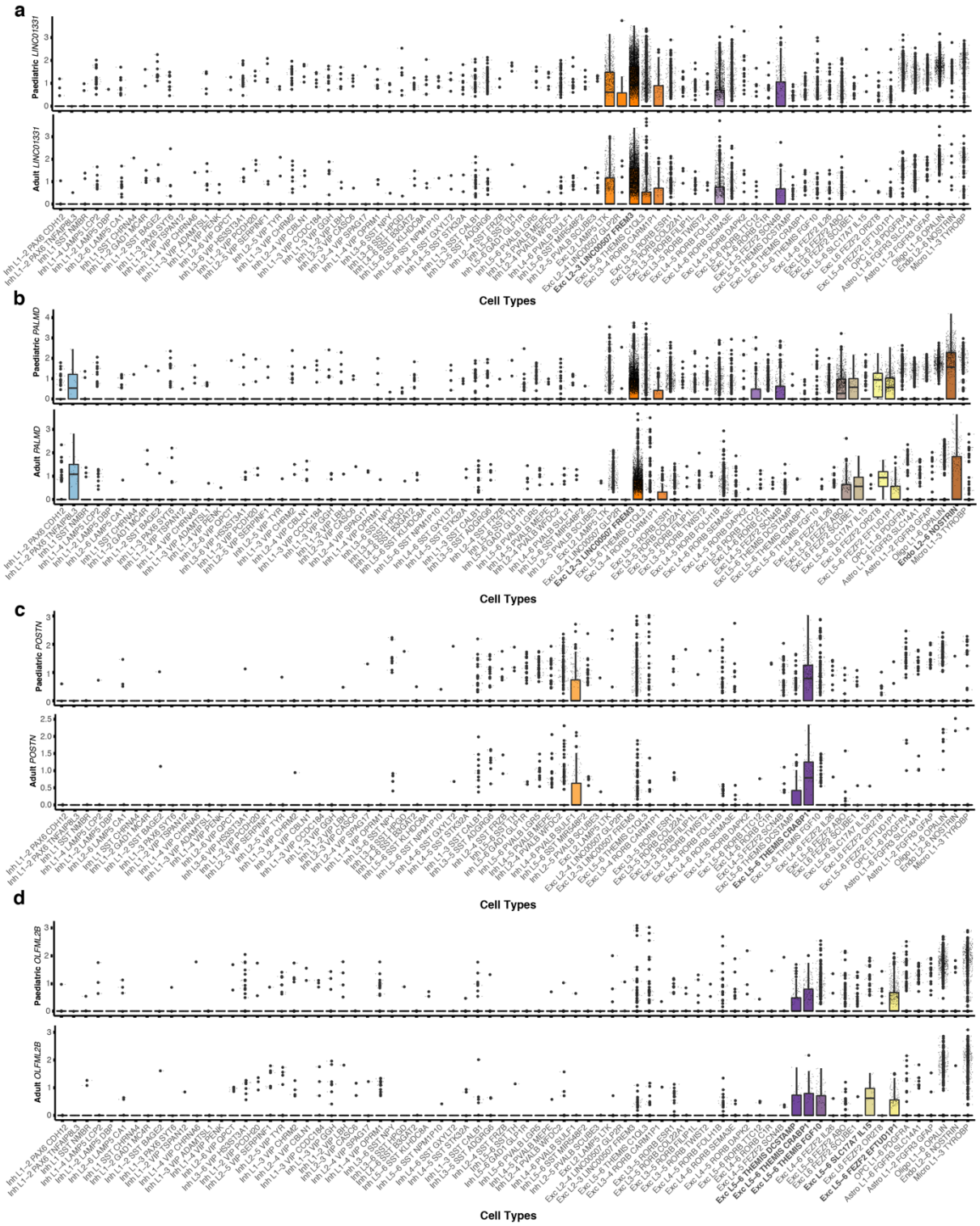

Extended Data Fig. 9: Evaluation of NS-Forest minimal marker gene expression across cell types in comparison to MTG cell taxonomy markers. a-d, Boxplots showing the normalised expression counts for *LINC01331* (**a**), *PALMD* (**b**), *POSTN* (**c**) and *OLFML2B* (**d**) in paediatric (top) and adult (bottom) datasets. The cell types expressing the markers at high levels are indicated in bold.

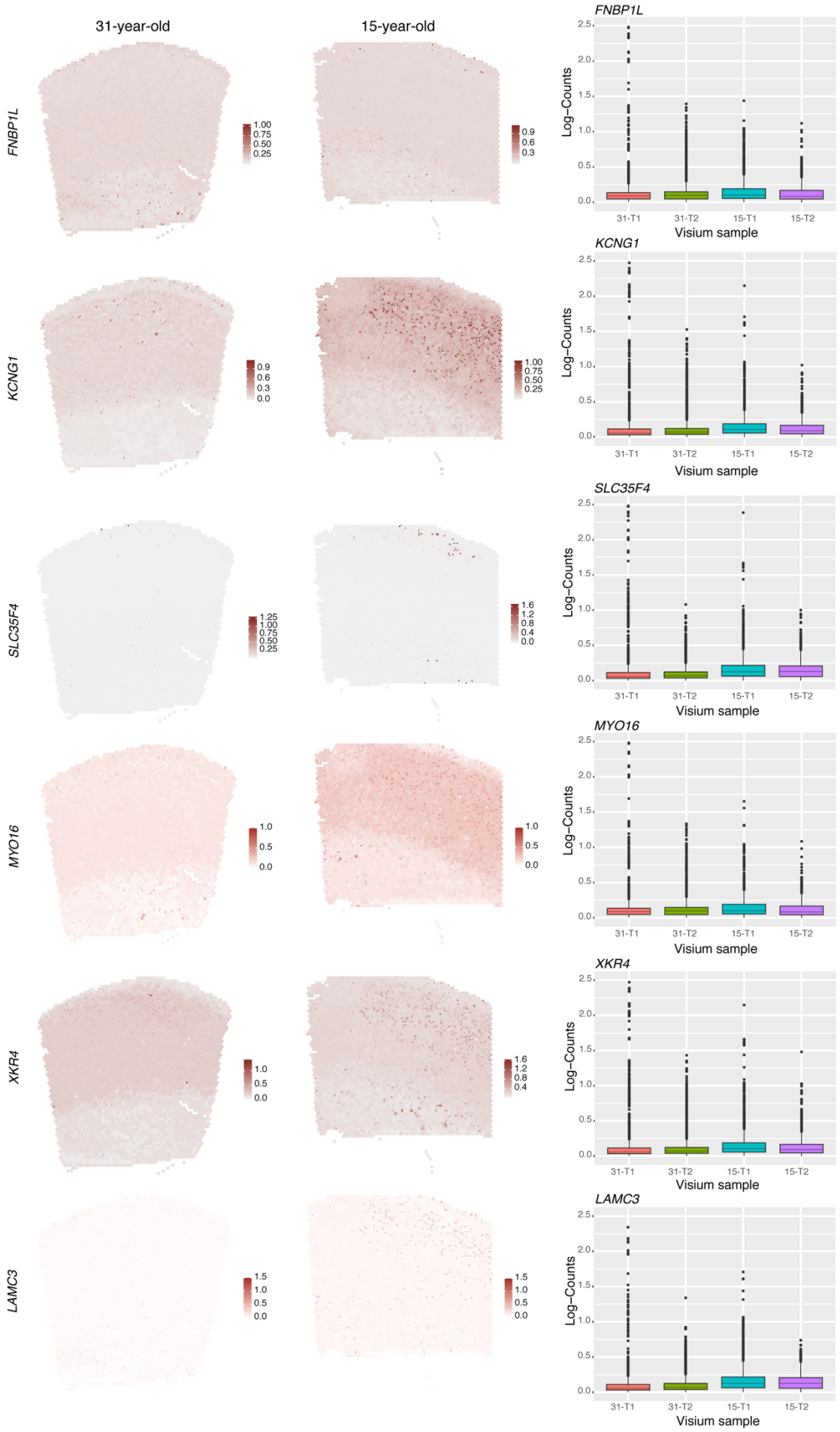

Extended Data Fig. 10: BayesSpace analysis of differentially expressed genes. High resolution Visium spatial gene expression profiles for selected DEGs using BayesSpace analysis to compare sub-spot level expression intensities between 31-year-old and 15-year-old temporal cortex tissue sections. Barplots show the average gene gene expression (log-counts) across technical replicate (T) samples for the indicated genes for spots with gene expression levels > 0. In all cases, average gene expression is higher in the 15-year-old samples than in the 31-year-old samples.

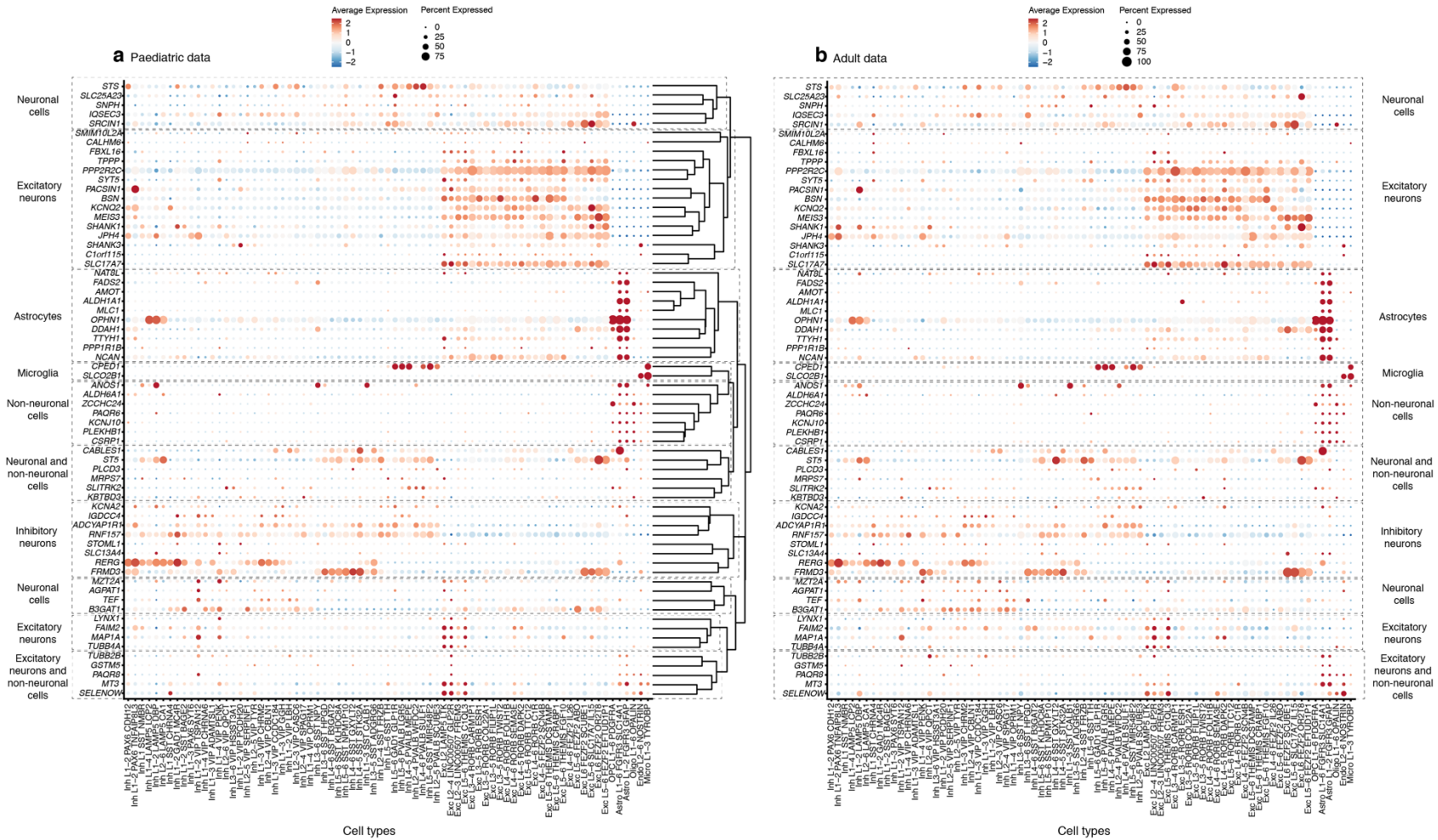

Extended Data Fig. 11: Cell type-specific expression of putative TBM biomarkers. **a**. Hierarchical clustering of TBM biomarker genes across the 75 cell types identified in the peaditaric snRNA-seq dataset reveals clusters of genes that are expressed by specific groups of cell types. **b**. Analysis of the same genes across the adult snRNA-seq dataset, using the gene order in (a) reveals very similar patterns of cell type-specific expression across the age-groups. Dashed boxes highlight gene clusters, with associated cell types indicated on the left and right of the right diagram

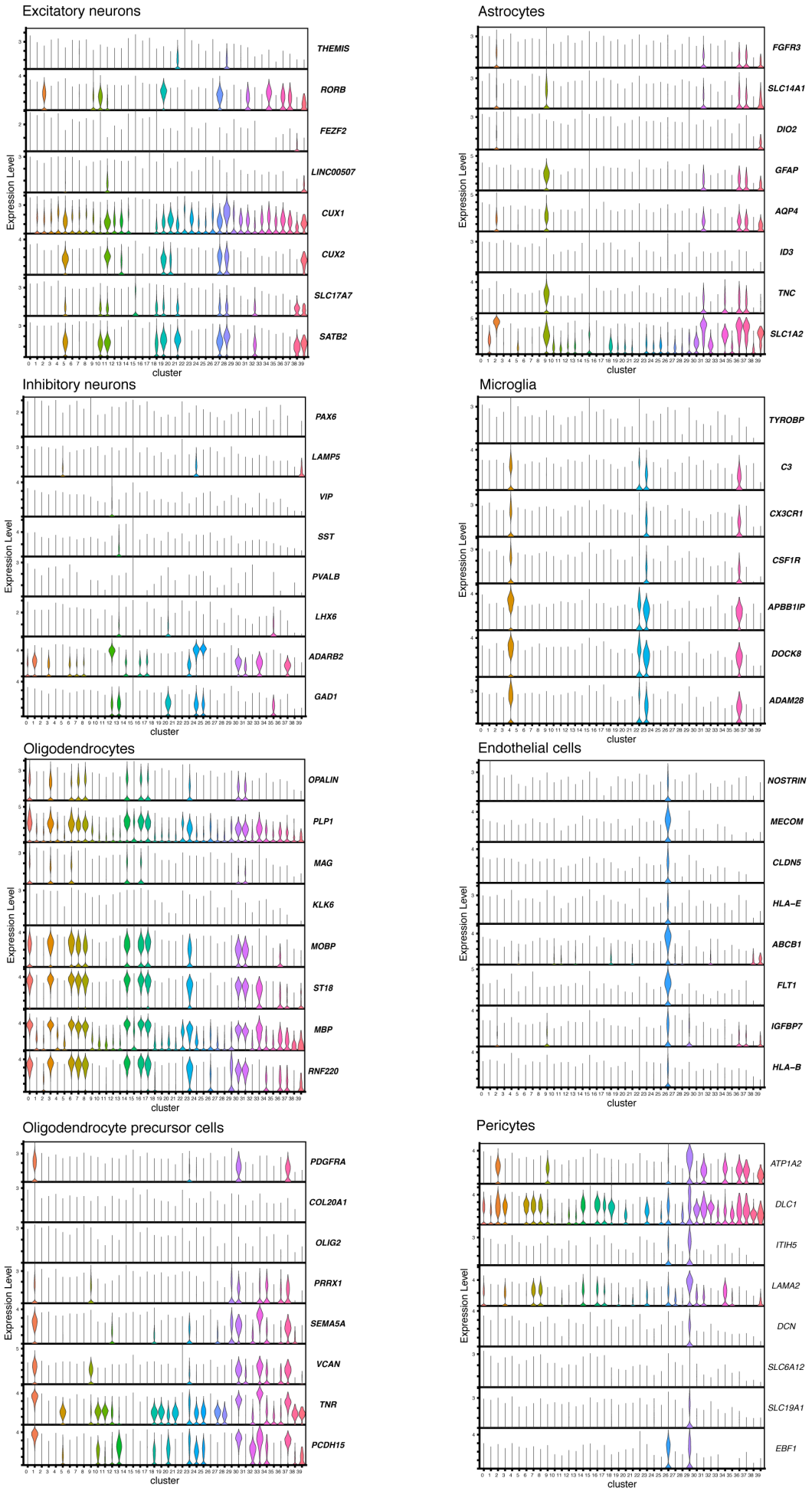

Supplementary Fig. 1: Violin plots showing the expression of known cell type marker genes across the Seurat clusters. These data were used for level 1 annotation of each cluster as one of the indicated major brain cell types (see also Extended Data Table 3).

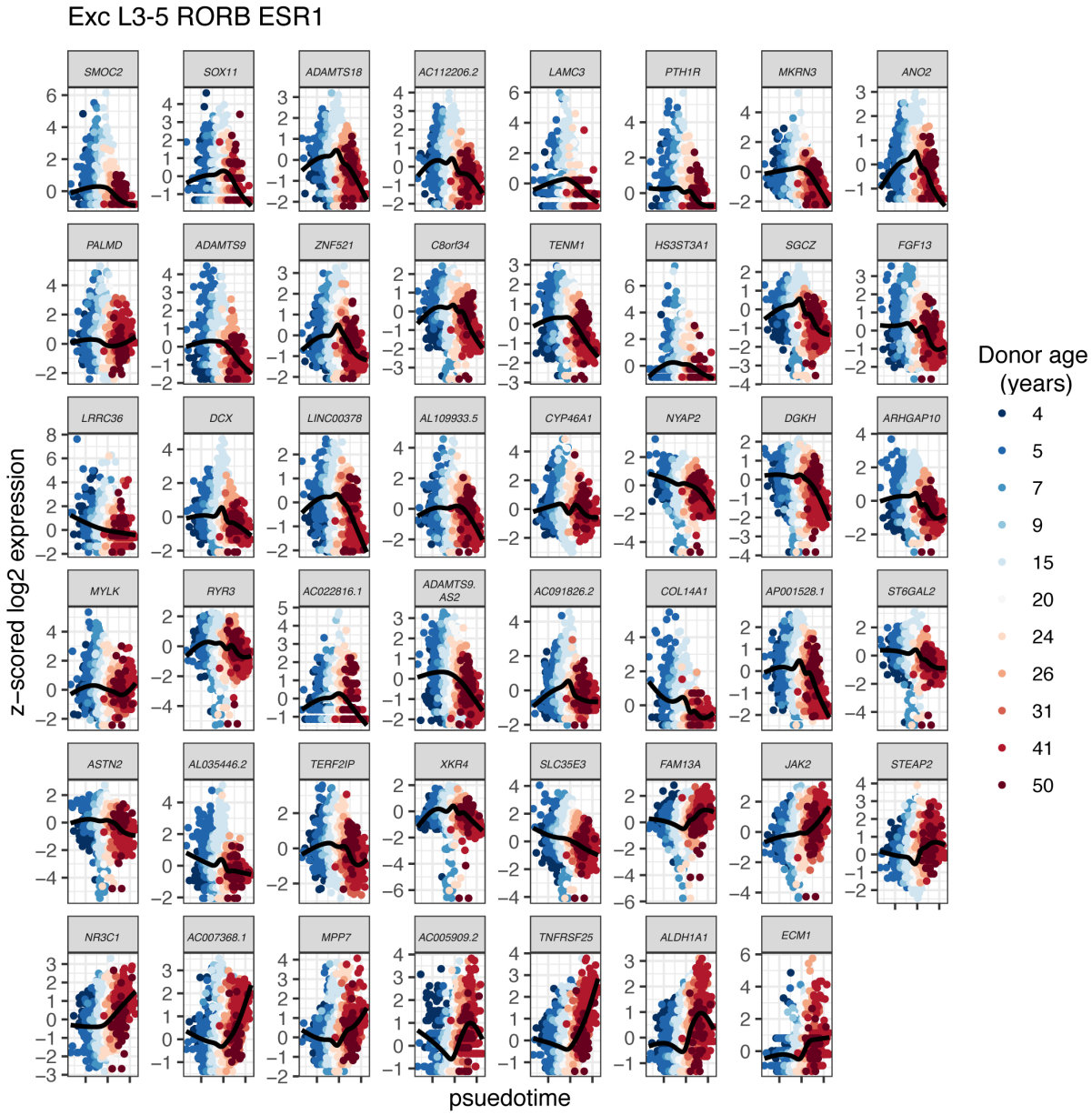

Supplementary Fig. 2: psupertime gene expression trajectories for all DEGs in Exc_L3-5_RORB_ESR1. The *x*-axis is the calculated psupertime value for each cell, coloured by sample of origin. The black lines are smoothened curves fit by geom_smooth in the R package ggplot2.

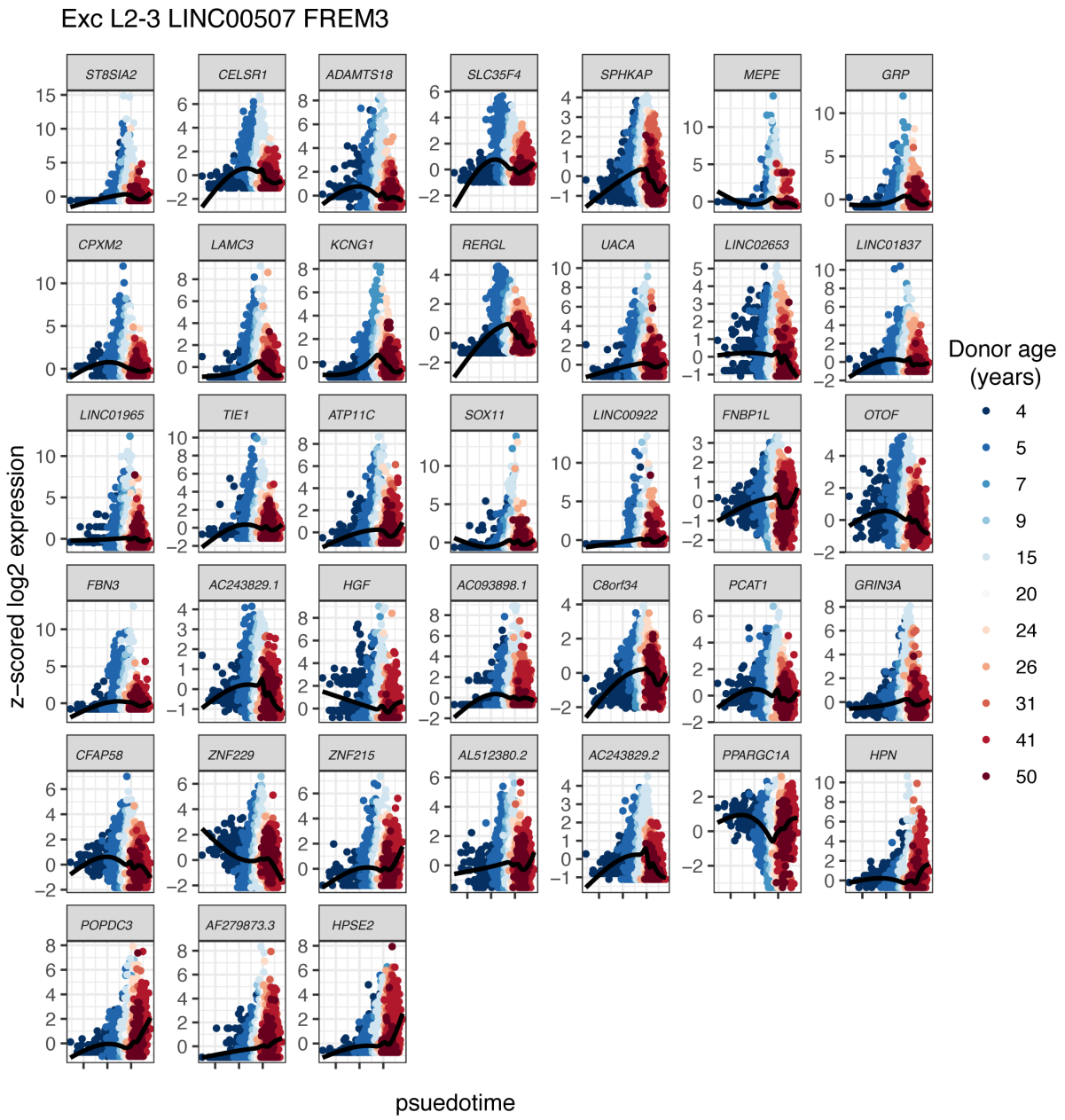

Supplementary Fig. 3: psupertime gene expression trajectories for all DEGs in Exc L2-3_LINC00507_FREM3. The *x*-axis is the calculated psupertime value for each cell, coloured by sample of origin. The black lines are smoothened curves fit by geom_smooth in the R package ggplot2.

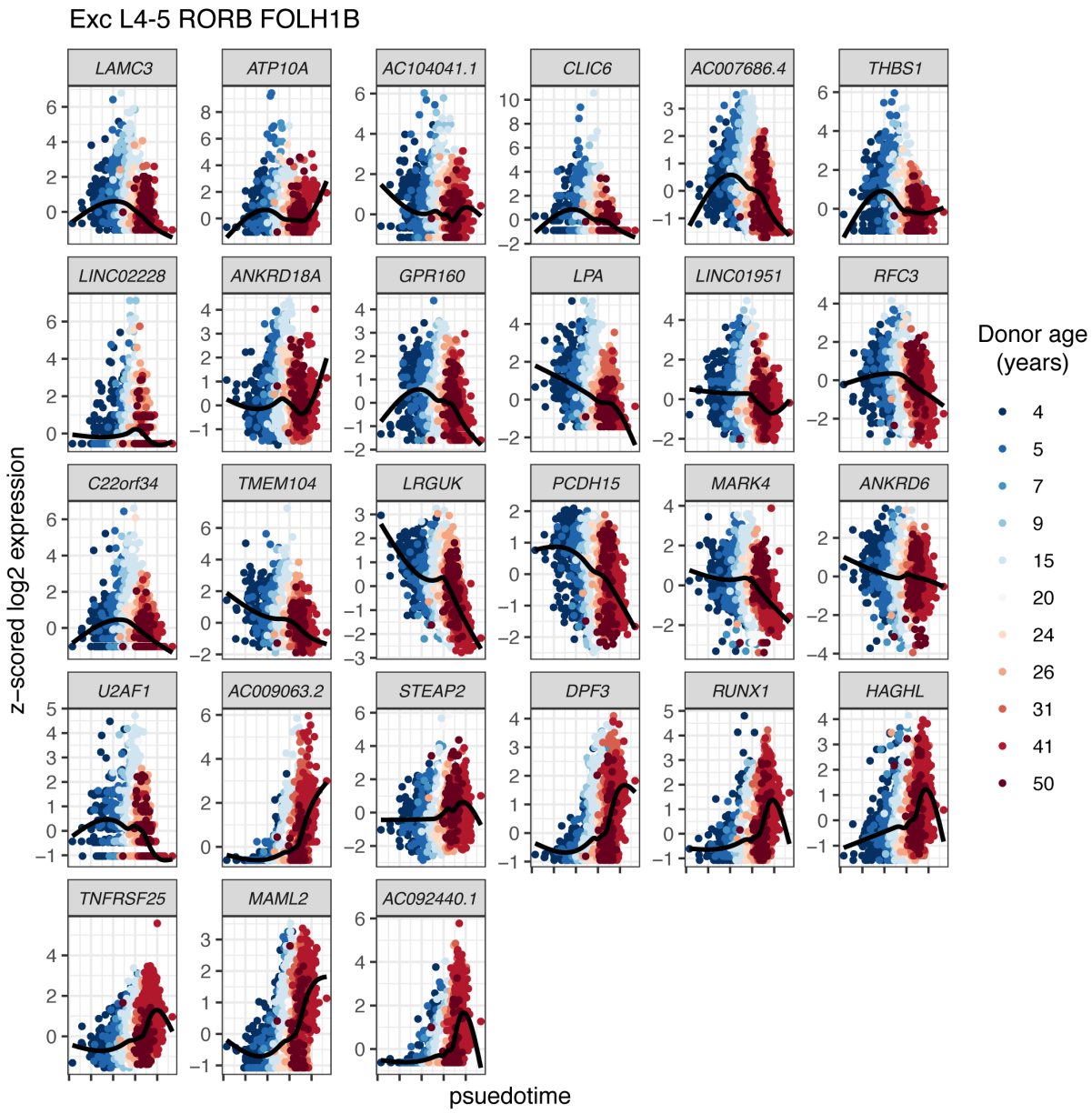

Supplementary Fig. 4: psupertime gene expression trajectories for all DEGs in Exc_L4-5_RORB_FOLH1B. The *x*-axis is the calculated psupertime value for each cell, coloured by sample of origin. The black lines are smoothened curves fit by geom_smooth in the R package ggplot2.

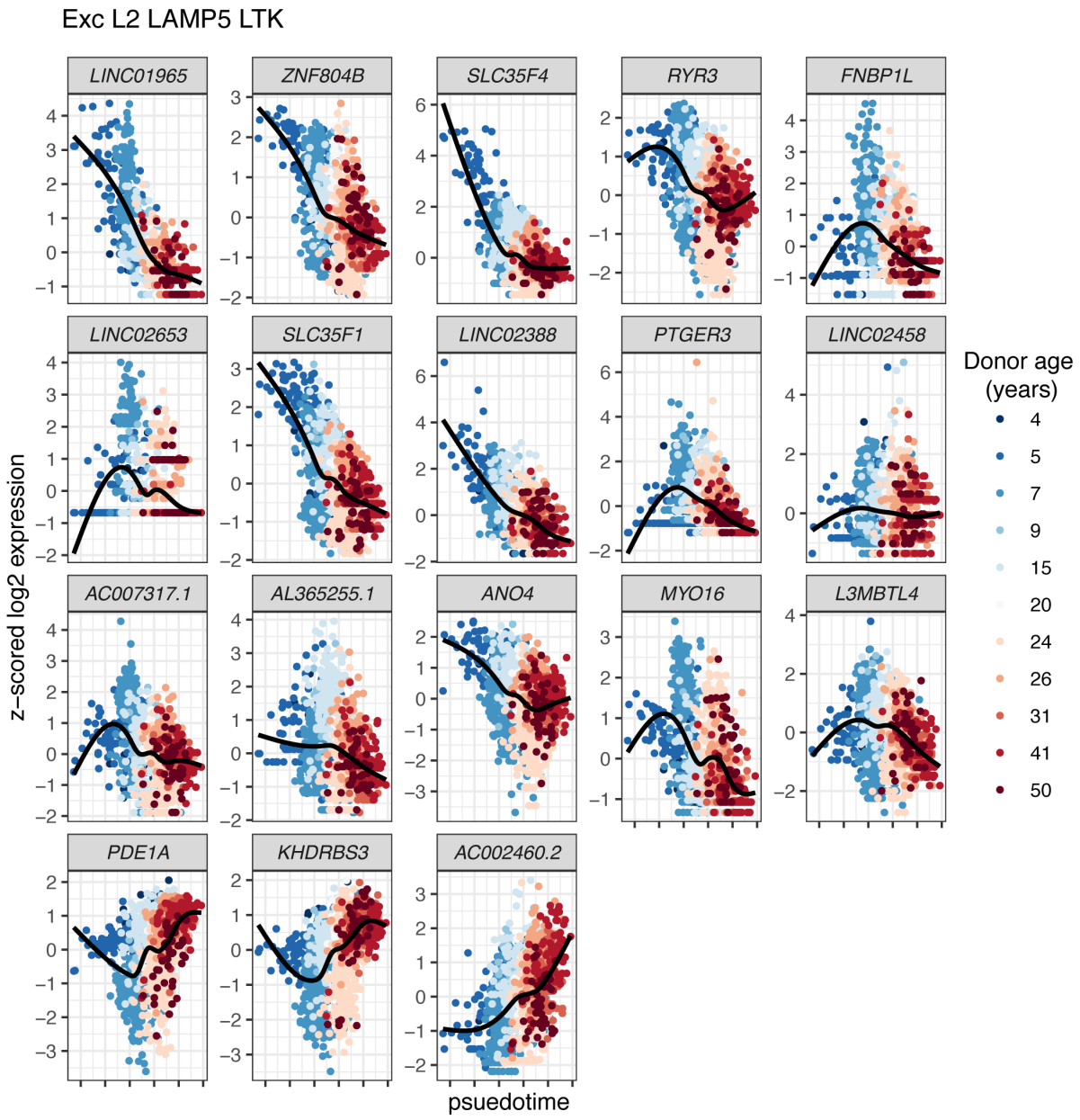

Supplementary Fig. 5: psupertime gene expression trajectories for all DEGs in Exc_L2_LAMP5_LTK. The *x*-axis is the calculated psupertime value for each cell, coloured by sample of origin. The black lines are smoothened curves fit by geom_smooth in the R package ggplot2.

Extended data Tables:

Extended Data Table 1: Summary of snRNA-seq, Visium and MERFISH sample metadata. Samples are ordered by age. The eight "P00" datasets were generated in the Hockman laboratory while the four "Nuc" datasets were generated by Thrupp et al. (2020)[24].

Extended Data Table 2: Summary of average quality control metrics for snRNA-seq datasets across nuclei for each sample before and after filtering. Several measures for quality control were evaluated on a per sample basis including the sequencing saturation, the mean number of reads per nucleus, the number of barcodes, the median number of genes detected per nucleus, the median number of UMIs detected per nucleus, and the number of doublets removed.

Extended Data Table 3: Label transfer annotation of snRNA-seq datasets using the Allen Brain Map MTG atlas as a reference. Sheet 1, Manual annotation of clusters into major cell types (level 1 annotation). **Sheet 2**, Number of nuclei per level 1 annotation category per sample. **Sheet 3**, Number of nuclei per MTG cell type per sample. The number of barcodes corresponding to each MTG cell type and sample is shown. Additionally, the total, minimum, and maximum number of nuclei per cell type and sample was computed. The number of cell types represented per sample was also determined. **Sheet 4**, Number of removed nuclei per level 1 annotation category per sample. **Sheet 5**, Number of removed nuclei per MTG cell type per sample. **Sheet 6**, Subtraction matrix comparing cosine similarity scores (i.e. similarity score for each cell subtype compared to the MTG cell Atlas as in Fig. 1d) for paediatric dataset to the adult dataset. Values are the paediatric scores minus the adult scores. **Sheet 7**, p-values, tests performed for each cell type and padj values (Benjamini-Hochberg method) when comparing the proportion of nuclei between male and female samples. **Sheet 8-10,** p-values, tests performed for each cell type and padj values (Benjamini-Hochberg method) when comparing the proportion of nuclei (sheet 8), number of genes (sheet 9; see Extended Data Fig. 3b) and number of UMIs (sheet 10; see Extended Data Fig. 3c) for each cell type between paediatric and adult samples shown.

Extended Data Table 4: Summary of average quality control metrics for Visium datasets. Several measures for quality control were evaluated on a per sample basis including the sequencing saturation, the percentage of read mapped to the transcriptome, the number of spots under the tissue, the average number of nuclei per spot determined by Vistoseg analysis, the mean reads detected per spot, the median genes detected per spot, the total number of genes detected, the median UMI Counts per Spot and the total number of nuclei.

Extended Data Table 5: NS-Forest minimal marker analysis. Sheet 1, Statistical tests evaluating the expression of Aevermann et al. (2021)[29] minimal markers (see their Supplementary Tables 1-2) in our datasets. **Sheets 2-3**, Metadata for each feature identified by NS-Forest marker in the down-sampled paediatric (**sheet 2**) and down-sampled adult (**sheet 3**) datasets describing the cell type, the F-beta score for each marker gene, overlap with Aevermann et al. (2021) and Hodge et al. (2019), uniqueness to the age group of interest, coding status, and uniqueness to the associated cell type as shown in Fig. 3. As input to NS-Forest, all datasets (six paediatric and six adult) were randomly down-sampled such that the total number of nuclei per sample was equal to the sample with the fewest number of nuclei.

Extended Data Table 6: gProfiler analysis of NS-forest markers. **Sheet1-3**, Significantly enriched GO terms associated with the paediatric (**sheet1**), adult (**sheet2**) and paediatric plus adult minimal marker genes identified by NS-forest. **Sheet3-5**, Significantly enriched GO terms associated with shared (i.e associated with both adult and paediatric samples) or paediatric-specific minimal marker genes with a binary expression score (> 0.7) for Oligo L1-6 OPALIN. Terms for which "highlighted" is true are driver terms.

Extended Data Table 7: Summary of metadata for NS-Forest markers with a binary expression score (> 0.7) per cell type across the paediatric and adult datasets. The number of shared markers, the number of markers unique to paediatric samples, and the number of markers unique to adult samples is shown for each cell type.

The number of nuclei per cell type is shown for the combined paediatric and adult down-sampled datasets, the down-sampled paediatric datasets, and down-sampled adult datasets.

Extended Data Table 8: Overlap NS-Forest markers with a binary expression score (> 0.7) per cell type between the paediatric and adult datasets. NS-Forest markers with a binary expression score (> 0.7) per cell type were extracted for the down-sampled paediatric and down-sampled adult datasets. Each sheet represents 1 of 75 cortical cell types and the NS-Forest features which were shared (intersect) between the paediatric and adult datasets, unique to paediatric datasets, or unique to adult datasets are shown.

Extended Data Table 9: DESeq2 output of all genes tested for differential expression between paediatric and adult brains per cell type. Sheet 1-75, Differential expression analysis was performed using DESeq2's Wald Test for each cell type separately. Genes were filtered prior to testing to only include those expressed in > 10% of nuclei for that cell type across all paediatric and adult datasets. The associated log2FoldChanges, p-adjusted values (padj, Benjamini-Hochberg method), and description of each feature are shown. Positive $\log_2$FoldChanges represent genes upregulated in paediatrics versus adults. See DESeq2 documentation for explanation of NA values (https://bioconductor.org/packages/release/bioc/vignettes/DESeq2/inst/doc/DESeq2.html#why-are-some-p-values-set-to-na).

Extended Data Table 10: DESeq2 output of significant DEGs only between paediatric and adult brains in a subset of cell types. Sheet 1-21, Significant DEGs (padj < 0.05) for cell types shown in Fig. 5a. The associated $\log_2$FoldChanges, p-adjusted values (padj), description, percentage of paediatric nuclei expressing the gene, percentage of adult nuclei expressing the gene, average normalised expression across paediatric nuclei, and average normalised expression across adult nuclei are shown. The difference in the peaditaric and adult values for percentage of nuclei and average normalised expression is also shown. Positive $\log_2$FoldChanges represent genes upregulated in paediatric versus adults datasets. See DESeq2 documentation for explanation of NA values (https://bioconductor.org/packages/release/bioc/vignettes/DESeq2/inst/doc/DESeq2.html#why-are-some-p-values-set-to-na). **Sheet 22-24**, EA (sheet 6), IQ (sheet7) and HAR (sheet8) associated DEGs and their associated cell types.

Extended Data Table 11: psupertime coefficients. The calculated psupertime coefficients for each gene for indicated excitatory neuron subtypes that showed the highest number of DEGs. Genes with non-zero psupertime coefficients represent genes that are relevant to the ordering of the cells in pseudotime.

Extended Data Table 12: **GSEA terms associated with each cell type showing enriched or depleted pathways in paediatric versus adult samples.** GSEA was performed using DESeq2's output gene lists for each cell type ranked according to the log2FoldChange*-$\log_2$(padj) for each gene. All DESeq2-tested genes served as input into GSEA (genes were expressed in > 10% of nuclei for the cell type of interest). Matrix shows the corresponding positive (**sheet 1**) and negative (**sheet 2**) NES values for each GSEA term (y axis) and cell type (x axis) based on the analysis using the ranked list of genes for each cell type. Terms were filtered to only include significantly associated terms ($p<0.01$, $q<0.1$). Positive NES values indicate pathways that are enriched in paediatric versus adult samples; negative NES values indicate pathways that are depleted in paediatric versus adult samples. The total number of terms per cell type and the total number of cell types associated with a given term are shown.